Geochemistry Geophysics Geosystems G3
AN ELECTRONIC JOURNAL OF THE EARTH SCIENCES
Published by AGU and the Geochemical Society

Article
Volume 10, Number 2
4 February 2009
Q02S11, doi:10.1029/2008GC002246
ISSN: 1525-2027

Galapagos-OIB signature in southern Central America: Mantle refertilization by arc–hot spot interaction

Esteban Gazel and Michael J. Carr
Department of Earth and Planetary Sciences, Rutgers University, 610 Taylor Road, Piscataway, New Jersey, 08854-8066, USA (egazel@rutgers.edu)

Kaj Hoernle
IFM-GEOMAR, Wischhofstrasse 1-3, D-24148 Kiel, Germany

Mark D. Feigenson
Department of Earth and Planetary Sciences, Rutgers University, 610 Taylor Road, Piscataway, New Jersey, 08854-8066, USA

David Szymanski
Department of Geological Sciences, Michigan State University, 206 Natural Science Building, East Lansing, Michigan, 48824-1115, USA

Folkmar Hauff and Paul van den Bogaard
IFM-GEOMAR, Wischhofstrasse 1-3, D-24148 Kiel, Germany

[1] Although most Central American magmas have a typical arc geochemical signature, magmas in southern Central America (central Costa Rica and Panama) have isotopic and trace element compositions with an ocean island basalt (OIB) affinity, similar to the Galapagos-OIB lavas (e.g., Ba/La < 40, La/Yb > 10, $^{206}Pb/^{204}Pb > 18.8$). Our new data for Costa Rica suggest that this signature, unusual for a convergent margin, has a relatively recent origin (Late Miocene ~6 Ma). We also show that there was a transition from typical arc magmas (analogous to the modern Nicaraguan volcanic front) to OIB-like magmas similar to the Galapagos hot spot. The geographic distribution of the Galapagos signature in recent lavas from southern Central America is present landward from the subduction of the Galapagos hot spot tracks (the Seamount Province and the Cocos/Coiba Ridge) at the Middle American Trench. The higher Pb isotopic ratios, relatively lower Sr and Nd isotopic ratios, and enriched incompatible-element signature of central Costa Rican magmas can be explained by arc–hot spot interaction. The isotopic ratios of central Costa Rican lavas require the subducting Seamount Province (Northern Galapagos Domain) component, whereas the isotopic ratios of the adakites and alkaline basalts from southern Costa Rica and Panama are in the geochemical range of the subducting Cocos/Coiba Ridge (Central Galapagos Domain). Geological and geochemical evidence collectively indicate that the relatively recent Galapagos-OIB signature in southern Central America represents a geochemical signal from subducting Galapagos hot spot tracks, which started to collide with the margin ~8 Ma ago. The Galapagos hot spot contribution decreases systematically along the volcanic front from central Costa Rica to NW Nicaragua.

Components: 11,853 words, 11 figures, 6 tables.

Keywords: Central America; Ocean Island Basalt; subduction; Galapagos hot spot; geochemistry; Sr-Nd-Pb isotopes.

Index Terms: 1031 Geochemistry: Subduction zone processes (3060, 3613, 8170, 8413); 1065 Geochemistry: Major and trace element geochemistry; 1040 Geochemistry: Radiogenic isotope geochemistry.

Received 15 September 2008; **Revised** 26 November 2008; **Accepted** 11 December 2008; **Published** 4 February 2009.

Gazel, E., M. J. Carr, K. Hoernle, M. D. Feigenson, D. Szymanski, F. Hauff, and P. van den Bogaard (2009), Galapagos-OIB signature in southern Central America: Mantle refertilization by arc–hot spot interaction, *Geochem. Geophys. Geosyst.*, *10*, Q02S11, doi:10.1029/2008GC002246.

Theme: Central American Subduction System
Guest Editors: G. Alvarado, K. Hoernle, and E. Silver

1. Introduction

1.1. Geotectonic Setting

[2] The Central American volcanic front extends parallel to the Middle American Trench from the Mexico-Guatemala border to central Costa Rica (Figure 1). The convergence rate between the Cocos and Caribbean plates increases to the southeast from ~60 mm/a off southern Guatemala to ~90 mm/a off southern Costa Rica [*DeMets*, 2001]. Smooth crust, produced at the East Pacific Rise spreading center, characterized by extensive trench-parallel structures [*Ranero et al.*, 2003] subducts to the north of the Nicoya Peninsula (Figure 1). The crust subducting to the south of the Nicoya Peninsula was produced at the relatively slow spreading Cocos-Nazca ridge (Figure 1). Much of this segment of subducting crust has been overprinted by Galapagos hot spot tracks. The Galapagos hot spot tracks in front of Costa Rica (Figure 1) range in age between 13.0 and 14.5 Ma [*Werner et al.*, 1999]. Active tectonic erosion has been reported in the Middle American Trench off Costa Rica [*Ranero and von Huene*, 2000; *Ranero et al.*, 2003]. The presence of a large province of accreted oceanic complexes along the Pacific coast of southern Central America suggest, however, that accretionary processes have also been important in the earlier evolution of this margin [*Denyer et al.*, 2006].

[3] The sediment cover of the Cocos Plate appears to be entirely subducted along most of the margin. The geochemical signature of the subducted sediment can be traced into the Central American volcanoes by Ba/La (Figure 2a). This ratio is particularly useful for Central America because it does not change significantly within the Cocos Plate sediment stratigraphy [*Patino et al.*, 2000]. Furthermore, since Ba/La correlates with $^{10}Be/^{9}Be$, the most definitive tracer of subducted sediment [*Leeman et al.*, 1994], it is a robust proxy to evaluate the sediment component. Along the volcanic front, the geochemical indicators of subducting sediments (e.g., Ba/La, U/Th, and $^{10}Be/^{9}Be$), define a slightly asymmetrical chevron pattern with a maximum in northwest Nicaragua [*Carr et al.*, 2003]. Higher La/Yb (steeper REE patterns) implies a lower degree of partial melting or derivation from a more enriched source. The overall correlation between La/Yb and Pb isotope ratios (Figures 2b and 2c) indicates that more enriched sources are present where La/Yb is higher (e.g., beneath Costa Rica and Guatemala). The mirror image in the along strike variations of La/Yb, Ba/La, and $^{206}Pb/^{204}Pb$ (Figures 2a–2c) suggests that the subducted sediment component, characterized by high Ba/La but low La/Yb and $^{206}Pb/^{204}Pb$ (probably in the form of a fluid) is dominant beneath Nicaragua and that an enriched OIB-type component, with low Ba/La but high La/Yb and $^{206}Pb/^{204}Pb$ (probably in the form of a melt), is dominant beneath Guatemala and central Costa Rica [*Eiler et al.*, 2005, *Hoernle et al.*, 2008, *Sadofsky et al.*, 2008].

[4] *Feigenson and Carr* [1993] proposed two mantle reservoirs for Central America. The most common reservoir is analogous to depleted mantle (DM) similar to the source of mid-ocean ridge basalt (MORB). The second reservoir has a more enriched composition and was visualized as veins within the DM reservoir. Melting of this veined mantle source and its interaction with the subduction component produced magmas with a typical arc signature [*Carr et al.*, 2003; *Feigenson et al.*, 2004]. This signature is dominant along most of the volcanic front; however, in central Costa Rica the lavas have an anomalous Galapagos-OIB signature [*Reagan and Gill*, 1989; *Herrstrom et*

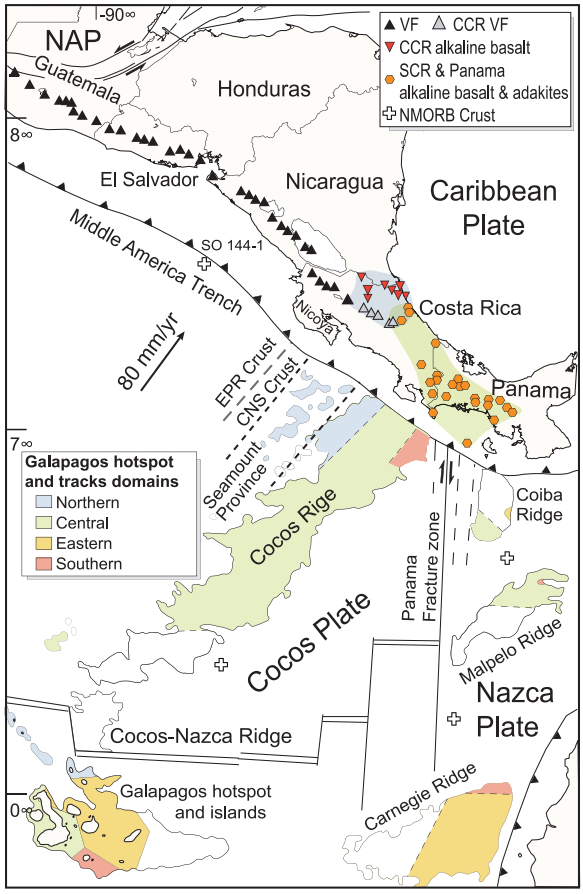

Figure 1. Tectonic setting of Central America [*Hoernle et al.*, 2008; *Alvarado et al.*, 2007; *Carr et al.*, 2003]. The Galapagos hot spot and tracks, both bathymetry and isotopic domains, are from *Hoernle et al.* [2000] and *Werner et al.* [2003]. Note that the isotopic compositions of the eruptive lavas in southern Central America match with the isotopic domains of the subducting Galapagos hot spot tracks in front of the trench. The central Costa Rican volcanic front lavas and alkaline basalts require the input of the subducting Seamount Province (Northern Galapagos Domain is shown by blue areas) and the southern Costa Rican and Panamanian adakites and alkaline basalts are in the range of the subducting Cocos and Coiba ridges (Central Galapagos Domain is shown by green areas) [*Hoernle et al.*, 2008, and this study]. CCR, central Costa Rica; CNS, Cocos-Nazca Spreading Center; EPR, East Pacific Rise; NAP, North American Plate; SCR, southern Costa Rica; VF, volcanic front.

al., 1995; *Gazel*, 2003; *Feigenson et al.*, 2004] (Figure 2).

[5] An array of often contradictory models exists to explain this anomalous OIB signature. *Herrstrom et al.* [1995] suggested that trench parallel flow above the subducting Nazca Plate proposed by *Russo and Silver* [1994] brings this enriched component from the mantle wedge beneath South America to the mantle wedge beneath southern Central America. *Abratis and Wörner* [2001] suggested that a "slab window" in the subducting Cocos Plate, proposed by *Johnston and Thorkelson* [1997], allowed Galapagos asthenosphere to rise through the window into the mantle wedge below southern Costa Rica and Panama. *Feigenson et al.* [2004] suggested that the OIB signature is the result of melting a Galapagos-modified mantle below central Costa Rica and Panama. *Goss and Kay* [2006] explained the OIB signature by incorporation of fore-arc oceanic complexes into the mantle wedge via tectonic erosion. *Benjamin et al.* [2007], *Hoernle et al.* [2008], and this study consider that this signature is derived from the Galapagos hot spot tracks subducting beneath Costa Rica and Panama.

1.2. Previous Work: Temporal Evolution of Arc Volcanism in Central America

[6] In contrast to the substantial international efforts to understand the active volcanic front, the temporal evolution of arc volcanism in Central America has been the focus of few studies. Miocene volcanic stratigraphy in Central America was compiled in El Salvador by *Wiesemann* [1975] and in Nicaragua by *Ehrenborg* [1996] and *Plank et al.* [2002]. In Costa Rica, there is evidence of arc volcanism in the sedimentary record since the Albian [*Calvo and Bolz*, 1994]. Nevertheless, the oldest in situ remnants of arc activity are the Sarapiquí Arc (22.2–11.4 Ma) [*Gazel et al.*, 2005], located behind the modern volcanic front of central Costa Rica (Figure 3). Older portions of the arc are also exposed in the Dominical area and the Talamanca Range (17.5–10.5 Ma) [*MacMillan et al.*, 2004] and the Aguacate Arc (11.35–4.04 Ma) [*Kussmaul et al.*, 1994; *MacMillan et al.*, 2004] (Figure 3). Normal arc volcanism ceased in the Talamanca area circa 14–11 Ma according to *MacMillan et al.* [2004], possibly as a result of the collision of older Galapagos hot spot tracks (e.g., Coiba Ridge) at this time with the Caribbean Plate [*Hoernle et al.*, 2008]. Subsequent volcanic activity in southern Costa Rica is represented by volumetrically minor adakitic-like suites. Although the term "adakite" is controversial [*Kelemen et al.*, 2003], we use it to refer to magmas interpreted to be derived through the melting of subducting oceanic crust within the garnet stability field, and the subsequent reaction of these melts with the mantle wedge, following the model of *Kay* [1978]. In the Talamanca Range, adakitic lavas <5 Ma are

exposed as individual domes or minor lava flows in the central part of the range and near the Panamanian-Costa Rican border [*Abratis and Wörner*, 2001; *MacMillan et al.*, 2004]. Their upper-mantle-like oxygen isotope ratios require mixing of slab melts from the upper low-temperature and lower high-temperature altered parts of the subducting crust [*Bindeman et al.*, 2005]. Slab melts in this part of the arc can be explained by melting of relatively young subducting Galapagos hot spot tracks (13.0–14.5 Ma) [*Werner et al.*, 1999] or by hot mantle upwelling [*Abratis and Wörner*, 2001].

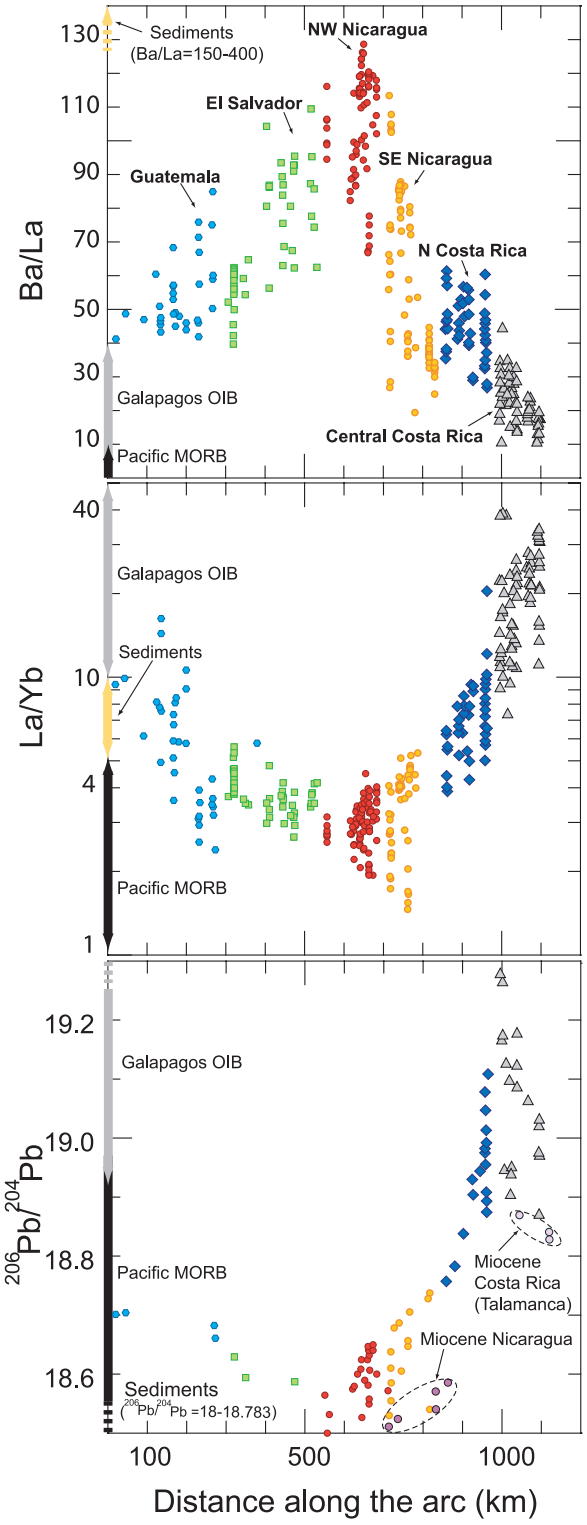

[7] The data presented here on the geochemical evolution of the Costa Rican arc allow us to test the different models that attempt to explain the origin of the Galapagos-OIB signature. We report major and trace element, isotopic and geochronological data that allow us to trace the geochemical evolution of magmas from Oligocene to Pliocene, and to explain the anomalous OIB signature as a result of the interaction of the arc with the subducting Galapagos hot spot tracks.

2. Samples and Analytical Methods

[8] Outcrops of Tertiary lavas and shallow intrusions were sampled from quarries, river beds, and road cuts following geologic maps of *Tournon and Alvarado* [1997] and *Gazel et al.* [2005]. We also sampled outcrops dated by *MacMillan et al.* [2004] (locations in Table 1). The objective was to elucidate the temporal geochemical evolution in Costa Rica in order to explain the anomalous OIB signature of the southern Central America magmas.

[9] Samples with no visible weathering, as verified by petrographic studies, were crushed in an alumina jaw crusher and washed with deionized water in an ultrasonic bath. Alteration-free rock chips (e.g., those free of oxides, veins, and zeolites) were selected under stereoscopic microscope and powdered in an alumina mill. Homogenous glass disks

Figure 2. Selected trace element and isotopic ratios for the different segments of the Central American volcanic front. The range of subducting sediments, Pacific MORB, and Galapagos hot spot lavas are plotted in the *y* axis for comparison. The maximum subducting sediment signal (Ba/La) is located in the NW Nicaragua segment and the minimum in central Costa Rica. The La/Yb and $^{206}Pb/^{204}Pb$ ratios of central Costa Rica are in range with the Galapagos OIB hot spot lavas while the rest of the arc show La/Yb and $^{206}Pb/^{204}Pb$ ratios in the range of a MORB source and subducting sediments. Data for the volcanic front from *Carr et al.* [2003], *Feigenson et al.* [2004], and *Hoernle et al.* [2008], for the subducting sediments from *Patino et al.* [2000], Pacific MORB and Galapagos hot spot data from Georoc database (http://georoc.mpch-mainz.gwdg.de).

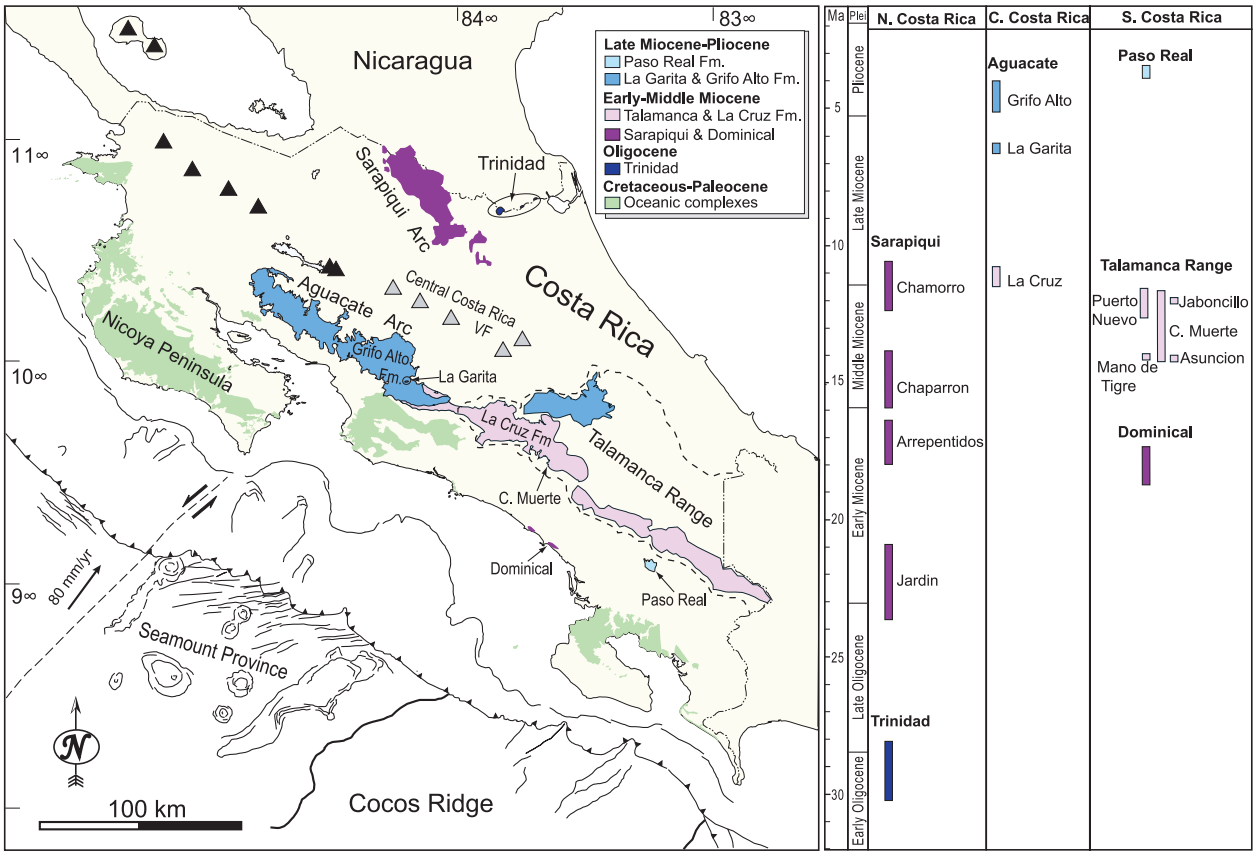

Figure 3. Simplified geologic map modified from *Denyer and Alvarado* [2007] that shows the different units sampled for this study. The locations of the samples are reported in Table 1. Bathymetric features from *Ranero and von Huene* [2000]. The chronostratigraphic range of the different units mention in the text and in Tables 1–3 is included to the right of the geologic map. Ages from *MacMillan et al.* [2004], *Gazel et al.* [2005], and this study. VF is volcanic front.

were produced at Michigan State University by fusing each powdered sample with lithium tetraborate ($Li_2B_4O_7$). Glass disks were then analyzed for major elements and selected trace elements (e.g., Cr, Cu, Ni, Sr, Rb, Zr, and Zn) by X-ray fluorescence (XRF) in a Bruker S4 Pioneer. Trace elements were obtained in the same glass disks by laser ablation inductively coupled plasma mass spectrometry (LA-ICP-MS) in a Micromass Platform ICP-MS with a Cetac LSX 200+ Nd:YAG laser (266 nm). The methods and precision are reported by *Hannah et al.* [2002].

[10] Sr-Nd-Pb isotope analyses were carried out on whole rock powders at the Department of Earth and Planetary Sciences, Rutgers University. About 100 mg of samples were weighed into a Teflon beaker and dissolved for 6 h (open beaker) in a 5:1 mixture of HF and HNO_3 at 150°C until the acids were volatilized. The sample were then redissolved in 3 ml of 0.5 N HNO_3 and centrifuged for 5 min. Sample digestion and element chromatography were performed in a Class 1000 clean room, equipped with Class 100 laminar flow hoods with downdraft exhaust. HCl, HF, and HNO_3 are Fisher Chemical trace metal grade acids, and ultrapure HBr is obtained from SEASTAR©. A Barnstead Nanopure II© purifying system provided 18.2 MΩ water.

[11] The ion-exchange chromatography followed established standard procedures [e.g., *Hart and Brooks*, 1974]. These include Pb separation using 30 μl Teflon microcolumns filled with BIORAD© AG 1x8 (100–200 mesh) resin that is equilibrated with 0.5 N HBr for highest Pb retention and from which Pb is released with 1 ml of 0.5 N HNO_3. The sample matrix collected during Pb chromatography (before the Pb is released) was then loaded in 1.5 N HCl onto 20 ml borosilicate glass columns filled with BIORAD© AG50W-X8 (100–200 mesh). Then the column loaded with 2.3 N HCl and 7.3 N HCl to separate Sr. The rare earth elements (REE) were obtained by loading 20 ml of 7.3 N HCl after Sr

Table 1. Geologic Units, Sample Locations, Ages, and Major and Trace Element Results[a]

Sample	Unit	Age (Ma)	Lat	Lon	Lit.	SiO_2	TiO_2	Al_2O_3	Fe_2O_3	MnO	MgO	CaO	Na_2O	K_2O	P_2O_5	Totals	LOI	Cr	Ni	Cu	Zn	Rb	Sr
											Trinidad												
P-125	Trinidad		10.7142	−83.9347	ba	52.43	0.9	19.26	9.14	0.16	3.9	9.86	2.71	0.66	0.2	99.33	0.81	30	18	76	71	11	388
P-126		29.20 ± 1.10	10.7252	−83.8855	ba	51.25	0.93	18.68	9.93	0.24	4.04	10.58	2.45	0.26	0.19	98.71	1.21	-	-	-	-	-	-
P-127		28.43 ± 0.10	10.7501	−83.8341	a	60.56	0.68	15.92	7.02	0.18	3.36	6.47	2.94	1.81	0.15	99.25	0.69	-	-	-	-	-	-
											Sarapiqui												
BT-020406-2	Jardin	22.20 ± 1.15*	10.6826	−84.2249	b	47.07	0.87	19.53	10.03	0.16	4.61	10.79	2.12	0.57	0.16	95.91	3.96	89	31	185	66	9	495
IN-020506-1			10.7872	−84.3425	b	49.36	0.98	17.84	10.06	0.16	4.81	9.29	2.63	1.00	0.24	96.37	3.50	110	41	152	73	18	471
IN-020506-2			10.7652	−84.2930	b	50.33	0.92	17.01	9.76	0.20	5.44	9.09	2.60	0.94	0.21	96.50	3.36	112	65	147	68	18	439
IN-020506-3			10.7872	−84.3425	b	50.65	1.01	17.88	10.58	0.19	4.95	9.58	2.70	1.02	0.25	98.81	1.05	102	44	143	74	21	467
IN-020506-5			10.7564	−84.2726	b	47.79	1.06	17.79	11.27	0.19	5.27	9.36	2.60	0.69	0.22	96.24	3.64	100	41	183	77	12	503
IN-020506-6			10.7566	−84.2718	b	49.35	1.15	17.54	12.24	0.22	5.25	9.52	2.78	0.77	0.24	99.06	0.82	97	38	190	81	15	497
IN-020506-7			10.7568	−84.2729	b	48.33	1.15	16.98	12.05	0.20	5.31	9.10	2.76	0.67	0.24	96.79	3.08	100	37	201	82	14	500
IN-020506-8			10.7729	−84.2749	b	48.07	0.89	18.63	8.72	0.18	3.38	8.87	2.68	0.86	0.21	92.49	7.38	-	-	-	-	-	-
IN-020806-1			10.7446	−84.2611	b	45.84	0.79	15.97	8.53	0.15	5.17	8.85	2.25	0.77	0.21	88.53	11.32	113	43	112	63	24	431
IN-020806-2			10.7702	−84.2214	b	44.17	0.62	20.68	7.69	0.15	4.17	11.19	1.82	0.49	0.14	91.12	8.78	131	44	96	51	8	523
IN-020806-3			10.7789	−84.2010	b	48.58	0.94	16.79	10.12	0.18	7.95	9.37	2.34	0.41	0.20	96.88	2.98	-	123	99	62	0	364
IN-020806-4			10.7739	−84.2115	b	46.19	0.70	20.88	7.99	0.19	4.61	11.55	1.98	0.52	0.16	94.77	5.11	137	46	108	53	7	521
IN-020806-5			10.7438	−84.2457	b	48.24	0.85	16.70	9.18	0.18	5.40	9.00	2.34	0.97	0.22	93.08	6.81	144	58	54	67	20	428
PS-020706-1			10.9108	−84.3835	b	47.19	0.88	18.14	9.52	0.18	4.39	9.63	2.55	0.55	0.19	93.22	6.66	95	34	156	69	6	468
PS-020706-2			10.9342	−84.3598	b	50.53	0.91	17.82	8.39	0.15	3.06	8.14	2.87	0.82	0.19	92.88	6.99	94	22	117	69	16	403
AR-020206-1	Arrepentidos	17.20 ± 0.80*	10.4598	−84.0283	b	49.27	1.01	19.37	10.09	0.22	3.74	9.61	2.83	0.74	0.21	97.09	2.77	-	27	201	74	12	494
AR-020206-2			10.4630	−84.0284	b	49.38	1.00	19.39	10.02	0.18	3.73	9.42	2.80	0.72	0.21	96.85	3.00	103	27	155	71	11	490
AR-020206-3			10.4688	−84.0297	b	49.60	1.00	18.25	9.90	0.34	4.31	9.78	2.61	0.81	0.22	96.82	3.04	114	38	117	70	13	439
AR-020206-4			10.4743	−84.0301	b	49.99	0.98	17.96	11.92	0.20	5.09	9.99	2.56	0.59	0.19	99.47	0.41	96	31	243	72	9	469
AR-020206-5			10.4770	−84.0331	ba	49.21	1.01	18.21	10.44	0.25	3.86	9.37	2.78	0.62	0.20	95.95	3.93	91	25	131	69	10	484
AR-020206-6			10.4791	−84.0358	ba	53.14	1.04	17.53	9.72	0.22	3.71	7.74	3.42	0.90	0.29	97.71	2.17	89	21	33	82	16	496
AR-020206-7			10.4905	−84.0399	ba	55.29	0.97	17.81	8.87	0.26	3.19	7.50	3.69	1.01	0.33	98.92	0.95	85	21	38	83	19	496
AR-020206-8			10.4655	−84.0084	ba	54.76	0.90	17.48	8.68	0.15	4.04	8.45	2.60	1.60	0.23	98.89	0.96	102	36	126	61	38	439
CH-020406-1	Chaparron	15.40 ± 0.6*	10.5501	−84.2084	ba	54.90	0.89	17.42	8.69	0.17	3.88	8.37	2.56	1.50	0.25	98.63	1.23	85	27	85	65	26	446
CH-020406-2			10.5501	−84.2084	ba	50.61	0.88	19.34	8.35	0.32	3.14	9.34	2.85	0.97	0.22	96.02	3.83	100	30	124	60	16	503
CH-020406-3			10.5501	−84.2084	ba	52.25	0.87	16.43	8.71	0.16	5.42	9.07	2.40	1.25	0.25	96.81	3.05	-	-	-	-	-	-
CH-020406-4			10.5501	−84.2084	ba	53.27	0.88	16.58	8.96	0.17	5.53	9.32	2.43	1.26	0.25	98.65	1.20	181	58	109	62	28	417
CH-020406-5			10.5831	−84.1805	ba	60.64	0.73	15.91	6.18	0.14	2.68	5.58	3.53	1.57	0.20	97.16	2.71	88	25	51	56	29	365
CH-020406-6			10.5392	−84.2192	a	55.54	0.90	17.45	8.26	0.17	3.83	8.34	2.57	1.48	0.25	98.79	1.07	-	-	-	-	-	-
BT-020406-3	Hito Sar		10.6859	−84.2116	ab	53.18	1.00	17.90	9.55	0.23	3.90	7.92	3.65	0.77	0.43	98.53	1.34	74	19	10	86	12	613
BT-020406-5			10.7316	−84.2032	di	50.49	0.69	15.42	10.00	0.17	9.02	10.77	1.95	0.35	0.11	98.97	0.93	372	105	111	60	6	262
BT-020406-6			10.7571	−84.1886	ab	48.64	0.85	16.83	10.45	0.17	7.40	9.74	2.30	0.45	0.17	97.00	2.86	270	103	112	112	6	363
BT-020406-7		-	10.6773	−84.2371	di	49.53	0.85	20.34	8.35	0.14	4.80	10.98	2.63	0.70	0.21	98.53	1.36	124	49	147	55	12	528
BT-020406-8			10.6683	−84.1970	ab	52.04	0.98	17.66	9.29	0.22	3.86	7.77	3.59	0.74	0.42	96.57	3.30	83	20	11	84	11	610
IN-020506-4			10.7522	−84.2918	ab	51.94	1.00	17.54	11.02	0.20	4.52	8.23	2.97	1.13	0.24	98.79	1.06	87	24	108	80	22	480
BT-020406-10			10.6683	−84.2417	di	48.14	0.96	17.93	10.50	0.18	5.10	9.93	2.46	0.58	0.20	95.98	3.91	95	35	161	73	11	470
BT-020406-9	Boca Tapada	-	10.6683	−84.2417	gb	52.17	1.13	15.84	10.34	0.19	3.59	7.25	3.33	1.19	0.31	95.34	4.53	83	26	154	79	22	407

Table 1. (continued)

Sample	Unit	Age (Ma)	Lat	Lon	Lit.	SiO_2	TiO_2	Al_2O_3	Fe_2O_3	MnO	MgO	CaO	Na_2O	K_2O	P_2O_5	Totals	LOI	Cr	Ni	Cu	Zn	Rb	Sr
PS-020706-3	Chamorro	11.40 ± 0.90*	10.9554	−84.3910	a	56.08	0.56	16.17	6.20	0.10	2.60	6.02	3.24	0.86	0.16	91.99	7.91	-	-	-	-	-	-
									Talamanca														
TA-021206-3	C. Asuncion	14.10 ± 1.0	9.5829	−83.7634	b	46.08	0.75	18.39	9.53	0.17	3.64	10.21	2.08	0.13	0.17	91.15	8.71	82	24	180	76	0	654
TA-021206-4			9.5761	−83.7604	ob	44.18	0.64	13.86	12.40	0.20	10.92	11.68	1.34	0.35	0.11	95.68	4.21	172	79	151	67	4	444
EG-1			9.5761	−83.7604	ob	-	-	-	-	-	-	-	-	-	-	-	-	93	53	105	74	4	513
TA-021206-6	C. Muerte	10.5 ± 0.9 to 13.00 ± 0.20**	9.5732	−83.9109	di	48.56	0.72	16.32	10.10	0.20	5.58	9.53	2.66	1.03	0.18	94.88	4.95	97	32	83	45	15	537
TC-1	C. Jaboncillo	11.98 ± 0.06**	9.6019	−83.7880	d	65.44	0.42	14.41	3.98	0.1	1.03	3.42	3.59	2.73	0.11	98.50	3.27	2	2	43	52	87	399
TC-2	C. Muerte	13.80 ± 0.9	9.4646	−83.7095	b (dike)	51.07	0.81	18.24	9.5	0.17	3.94	8.94	2.41	0.64	0.16	98.73	2.85	7	6	96	72	8	572
TC-4	Mano de Tigre	14.1 ± 0.15**	9.0320	−83.2911	b	47.73	0.86	20.56	10.68	0.19	3.98	11.19	2.3	0.51	0.15	99.09	0.94	3	6	140	80	4	545
TC-9	Puerto Nuevo Fm.	11.76 ± 0.12**	8.9650	−83.4374	b (dike)	-	-	-	-	-	-	-	-	-	-	-	-	8	11	212	45	33	686
									Paso Real														
GE-021306-4	Paso Real Fm.	3.59 ± 0.06 to	9.0730	−83.2916	a	56.16	0.63	17.05	6.30	0.11	3.48	6.59	3.26	2.24	0.26	96.08	3.66	93	38	167	58	37	1014
GE-021306-5		3.65 ± 0.30**	9.0730	−83.2916	b	46.12	0.75	18.60	10.37	0.25	5.17	9.31	2.40	1.80	0.46	95.23	4.53	76	26	197	72	41	941
GE-021306-6			9.0657	−83.2902	b	47.04	0.72	17.03	9.73	0.20	5.51	9.05	2.55	1.51	0.32	93.66	6.10	98	36	177	70	22	988
GE-021306-7			9.0426	−83.3004	ba	55.82	0.63	17.65	6.69	0.12	3.34	6.82	3.30	1.83	0.25	96.45	3.32	82	30	152	63	28	892
GE-021306-8			9.0369	−83.2868	ba	51.62	0.67	18.01	8.45	0.17	4.02	8.16	3.07	1.67	0.36	96.20	3.52	94	30	210	76	24	1105
GE-021306-9			9.0650	−83.3179	ba	44.16	0.87	16.51	10.25	0.22	6.00	9.96	2.27	1.51	0.39	92.14	7.51	99	33	220	74	8	1629
GE-021306-10			9.0803	−83.2834	ba	49.09	0.78	18.01	9.66	0.18	4.96	9.50	2.73	1.22	0.29	96.42	3.36	82	29	207	72	15	1028
									Dominical														
DO-021406-1	Dominical	17.50 ± 0.10**	9.2061	−83.8015	gb	44.15	1.12	15.28	12.09	0.17	4.62	9.21	2.68	1.02	0.19	90.53	9.30	99	27	490	68	17	417
DO-021406-2			9.1399	−83.7208	gb	44.78	0.77	19.72	9.56	0.16	4.00	10.75	2.10	0.59	0.13	92.56	7.30	93	28	242	74	7	556
TC-10a		18.32 ± 0.32**	9.1358	−83.7177	a (dike)	-	-	-	-	-	-	-	-	-	-	-	-	2.33	7	390	119	30	477
									Aguacate														
CA-021106-1	La Cruz Fm.	10.90 ± 0.10–	9.7944	−84.2116	b	45.73	0.86	18.03	10.79	0.17	6.00	11.64	2.02	0.47	0.15	95.86	3.98	95	47	195	63	4	528
CA-021106-2		11.35 ± 0.10**	9.7930	−84.2344	ba	49.87	1.45	14.13	13.34	0.31	3.60	7.47	3.09	0.94	0.28	94.48	5.34	106	21	157	114	13	376
CA-021106-3			9.7932	−84.2385	ab	49.17	1.43	14.31	13.21	0.25	3.61	7.12	3.02	0.94	0.28	93.34	6.47	75	20	143	112	13	374
CA-021106-4			9.8027	−84.1934	b	49.40	0.70	17.58	9.45	0.18	5.17	10.53	2.22	0.84	0.12	96.19	3.65	106	39	168	60	15	479
CA-021106-5	Grifo Alto Fm.	5.10 ± 0.10–	9.8507	−84.3799	b	47.03	0.80	19.03	10.84	0.18	4.92	10.31	2.37	0.73	0.24	96.45	3.38	96	32	158	67	10	802
CA-021106-6		4.04 ± 0.04**	9.8507	−84.3799	ba	49.62	0.84	19.40	10.34	0.20	3.97	10.03	2.62	0.98	0.27	98.27	1.54	83	22	172	70	15	850
CA-021106-7			9.8589	−84.3813	ba	48.58	0.85	19.23	10.80	0.20	4.67	9.90	2.60	0.94	0.32	98.09	1.70	89	29	152	70	12	883
CA-021106-8			9.8756	−84.3842	ba	49.91	0.75	18.28	10.31	0.18	5.08	9.85	2.72	1.04	0.22	98.34	1.41	-	-	-	-	-	-
ACZ			10.0864	−84.4360		51.78	0.82	18.26	9.34	0.18	3.93	8.81	3.09	1.98	0.42	98.61	1.13	-	-	118	69	37	980
CLC-1			10.0570	−84.4556	b	50.99	0.87	18.78	8.93	0.15	4.11	9.87	2.62	1.83	0.30	98.45	1.28	-	-	177	65	28	1228
CC-1			10.0406	−84.4142	b	49.95	0.85	18.18	9.53	0.17	4.41	9.97	2.45	2.21	0.38	98.10	1.63	-	-	14	66	40	1046
CC-2			10.0406	−84.4142	b (dike)	49.13	0.84	18.14	9.86	0.17	4.59	9.70	2.38	2.16	0.38	97.35	2.36	-	-	244	69	38	1046
CA-1			10.0272	−84.4072	b	51.77	0.82	18.61	9.13	0.18	3.71	8.84	3.05	2.00	0.43	98.54	1.22	-	-	122	68	36	992
FR-1			10.0524	−84.4584	b	51.06	0.82	18.10	9.93	0.19	4.51	9.33	2.62	1.49	0.25	98.30	1.50	-	-	146	66	29	813
SM-1			10.0660	−84.4123	a	55.16	0.64	14.78	6.19	0.14	5.51	8.21	2.91	2.30	0.50	96.34	3.35	177	89	97	52	56	1106

Table 1. (continued)

Sample	Unit	Age (Ma)	Lat	Lon	Lit.	SiO_2	TiO_2	Al_2O_3	Fe_2O_3	MnO	MgO	CaO	Na_2O	K_2O	P_2O_5	Totals	LOI	Cr	Ni	Cu	Zn	Rb	Sr
LG-040105-1	La Garita Fm.		9.9879	−84.3467	ob (sill)	43.06	1.10	14.89	12.90	0.19	8.37	12.11	2.26	0.65	0.33	95.86	3.87	79	70	152	74	25	1393
LG-040105-2			9.9879	−84.3467	b (dike)	49.49	1.05	17.83	10.30	0.24	3.90	8.62	3.22	2.30	0.49	97.44	2.31	-	-	165	76	42	905
LC-010405-3			10.0739	−84.4509	b	46.85	0.86	17.53	11.19	0.17	6.71	11.37	1.89	1.21	0.26	98.04	1.77	-	-	90	63	20	861
LC-1			10.0725	−84.4511	b (dike)	44.63	0.92	16.20	12.45	0.21	8.68	11.55	1.84	0.91	0.49	97.88	1.88	79	30	190	73	36	1095
P-95		6.47 ± 0.21	9.9865	−84.3446	ob (sill)	46.18	1.03	17.87	11.46	0.19	6.46	10.73	2.33	1.28	0.29	98.06	1.79	35.66	38	173	85	30	869
									Standards														
JB-1a						51.68	1.25	14.20	8.80	0.14	7.78	9.17	2.66	1.40	0.26	97.34	2.47	336	134	54	69	36	428
JB-1a						51.91	1.27	14.32	8.87	0.15	7.84	9.25	2.67	1.41	0.26	97.95	1.86	356	136	62	69	37	435
JB-1a						52.05	1.26	14.25	8.87	0.14	7.83	9.24	2.63	1.41	0.26	97.94	1.89	331	136	63	69	37	435
JB-1a						51.77	1.24	14.15	8.79	0.14	7.78	9.16	2.62	1.40	0.27	97.32	2.5	327	133	53	68	37	430

[a] Asterisk indicates ages from *Gazel et al.* [2005]; two asterisks indicate ages from *MacMillan et al.* [2004]. Additional data and plateaus for the new $^{40}Ar/^{39}Ar$ ages are found in Appendix A. Lit, lithology; a, andesite; ab, aphyric basalt; b, basalt; ba, basaltic andesite; d, dacite; di, diabase; gb, gabbro; ol, olivine-rich basalt.

collection. The solution containing REE was then loaded in 0.23 N HCl onto 4 ml quartz glass columns filled with HDEHP-Teflon resin to separate the Nd from the other REE. There is a 100% separation of Sm from Nd with this technique, but with significant contamination of the Nd fraction with Ce, requiring analysis of Nd metal rather than Nd oxide during mass spectrometer runs.

[12] Isotopic ratios were determined by thermal ionization mass spectrometry (TIMS) at the Department of Earth and Planetary Sciences at Rutgers University on a GV Isoprobe-T multicollector. Sr and Nd are measured in dynamic multicollection mode, whereas Pb is measured in static multicollection. Sr and Nd isotopic ratios are normalized within each run to $^{86}Sr/^{88}Sr = 0.1194$ and $^{146}Nd/^{144}Nd = 0.7219$, respectively, and all errors are reported as 2 sigma of the mean. Reference material measured along with the samples gave $^{87}Sr/^{86}Sr = 0.710241 \pm 0.000006$ (n = 33) for NBS987 and $^{143}Nd/^{144}Nd = 0.511851 \pm 0.000006$ (n = 20) for La Jolla standards. The reproducibility of NBS 981 (n = 13) is $^{206}Pb/^{204}Pb = 16.896 \pm 0.009$, $^{207}Pb/^{204}Pb = 15.437 \pm 0.013$, $^{208}Pb/^{204}Pb = 36.541 \pm 0.011$. Pb isotope ratios were normalized to NBS 981 values of *Galer and Abouchami* [1998]. Total chemistry blanks are <100 pg for Sr, Nd, and Pb and are thus considered negligible for the amount of sample processed.

[13] A subset of 10 samples (codes EG-, P-, and TC-; Tables 1, 2, and 3) were analyzed at IFM-GEOMAR and the University of Kiel. Samples were first crushed to small pieces, then washed in deionized water and carefully hand-picked under a binocular microscope. Major elements and some trace elements (e.g., Cr, Ni, Zr, Sr) of whole rock samples were determined on fused beads using a Philips X'Unique PW1480 X-ray fluorescence spectrometer (XRF) equipped with a Rh-tube at IFM-GEOMAR. H_2O and CO_2 were analyzed in an infrared photometer (Rosemount CSA 5003). Additional trace elements (e.g., Rb, Ba, Y, Nb, Ta, Hf, U, Th, Pb, and all REE) were determined by ICP-MS on a VG Plasmaquad PQ1-ICP-MS at the Institute of Geosciences (University of Kiel) after the methods of *Garbe-Schönberg* [1993]. Pb isotopes were determined in a Finningan MAT 262-RPQ^{2+}, Sr and Nd isotopes in a ThemoFinnigan TRITON TIMS at IFM-GEOMAR. The procedures and precision are detailed in the work of *Geldmacher et al.* [2006] and *Hoernle et al.* [2008]. Interlab comparison can be made with the

samples TA-021206-4 analyzed by the Rutgers-Michigan State Labs and EG-1 analyzed at the IFM-GEOMAR labs. Even though the codes are different, this sample was collected by the first author in the same place and split for different lab analyses. For this particular sample (EG-1/TA-021206-4) the different lab results are in good agreement within the analytical errors (Tables 1, 2, and 3).

[14] Key samples were dated by step-heating $^{40}Ar/^{39}Ar$ to compliment the existing geochronology record reported in the literature [*MacMillan et al.*, 2004; *Gazel et al.*, 2005] (Table 1). Mineral separates, rock matrix samples, and irradiation monitor TCR-2 (sanidine from Taylor Creek Rhyolite; Age = 27.87 Ma) [*Lanphere and Dalrymple*, 2000] were irradiated in position E6 of the FRG-1 nuclear reactor at the GKSS Research Center, Geesthacht, using a Cd shielding. Step-heating $^{40}Ar/^{39}Ar$ analyses were carried out with a 20 W argon-ion laser in a MAP 216 mass spectrometer at IFM-GEOMAR. Analysis of system blanks were measured prior to each sample and after each fifth sample heating step, typically comprising 10%, 1%, and 2% of the measured ^{36}Ar, ^{39}Ar, and ^{40}Ar isotopes, respectively. The data reported included more than 50% of ^{39}Ar in each plateau.

3. Data and Results

[15] The main crystalline phases in the Oligocene-Middle Miocene samples are zoned plagioclase and clinopyroxene. Olivine is present in the basalts and basaltic andesites, typically altered to chlorite or iddingsite. Matrix textures in the lavas range from trachytic to interstitial and are composed of plagioclase, pyroxene, and magnetite. In general, the Oligocene-Middle Miocene samples display some degree of low temperature alteration (chlorite + zeolites). The petrography shows only one major temporal change, the appearance of orthopyroxene as a phenocryst phase during the Late Miocene.

[16] We report 76 new major element analyses and 72 new trace element analyses presented in Tables 1 and 2. The analyzed samples include basalts, basaltic-andesites, some andesites, and one dacite (Figure 4). The Oligocene-Middle Miocene samples belong to the calc-alkaline series, similar to the Nicaraguan volcanic front lavas, whereas most of the Late Miocene-Pliocene samples belong to the high-K calc-alkaline to transitional shoshonitic series, similar to the Central Costa Rican volcanic front lavas (Figure 4). With the exception of lower Ba, Th, U, and Pb, the Oligocene-Middle Miocene rocks are very similar to lavas from the Nicaraguan volcanic front and have more depleted compositions than lavas from the central Costa Rica volcanic front (Figure 5). The Late Miocene-Pliocene samples have incompatible-element abundances closer the central Costa Rica volcanic front lavas (Figure 5).

[17] The Sr-Nd-Pb isotopes data are presented in Table 3. The radiogenic isotope ratios were age-corrected [*Faure*, 1986] assuming that ages reported in the literature or in this study (Table 1) apply uniformly within each geologic unit. The corrected isotopic ratios in Table 3 are plotted in Figures 6, 7, and 9. The most radiogenic Pb isotopic ratios occur in the Late Miocene-Pliocene units (e.g., $^{206}Pb/^{204}Pb > 18.8$ and $^{208}Pb/^{204}Pb > 38.5$; Figure 6). $^{87}Sr/^{86}Sr$ increased from 0.7035 in the Oligocene samples to 0.7042 in the Middle Miocene samples and decreased to 0.7035 in the Late Miocene-Pliocene units. $^{143}Nd/^{144}Nd$ increased from 0.51298 in the Oligocene to 0.51302 in Middle Miocene and decreased to 0.51295 by Late Miocene-Pliocene (Figure 6).

[18] New $^{40}Ar/^{39}Ar$ step-heating ages are reported in Table 1. Analytical data and age spectrum are provided in the supplementary material (Appendix A). The new ages from the Trinidad area (Figure 3) (sample P-126 matrix and sample P-217 plagioclase separate) are the oldest reliable $^{40}Ar/^{39}Ar$ ages for in situ remnants of arc magmatism in Costa Rica and range from 28.4 ± 0.42 to 29.2 ± 0.1 Ma. The oldest $^{40}Ar/^{39}Ar$ age previously reported from the intrusives of the Dominical area was 17.5 ± 0.10 Ma, (Figure 3) [*MacMillan et al.*, 2004]. A new $^{40}Ar/^{39}Ar$ age (plagioclase separate) from an andesitic dike from this area provides a slightly older age of 18.3 ± 0.3 Ma. The matrix of a diabase from the Cerro de la Muerte area (Figure 3) yields an $^{40}Ar/^{39}Ar$ age of 13.77 ± 0.43 Ma and the matrix from a nearby olivine basalt yields an age of 14.1 ± 1.0 Ma. Both of these ages are in agreement with the ones published by *MacMillan et al.* [2004] for volcanic and subvolcanic rocks from the Talamanca Range in this area. The matrix from a basaltic sill from the La Garita Formation (Figure 3) yielded a $^{40}Ar/^{39}Ar$ age of 6.47 ± 0.21 Ma. The locations of these geologic units are show in Figure 3.

4. Discussion

[19] The new major observation reported here is the temporal magmatic evolution in Costa Rica. We first describe the geochemical changes over

Table 2. ICP-MS Trace Element Results

Sample	V	Y	Zr	Nb	Ba	La	Ce	Pr	Nd	Sm	Eu	Gd	Tb	Dy	Ho	Er	Yb	Lu	Hf	Ta	Pb	Th	U
										Trinidad													
P-125	261.22	22.65	65.57	2.77	227.72	6.93	15.36	2.56	11.85	3.19	1.02	3.62	0.61	3.89	0.81	2.32	2.43	0.37	1.78	0.17	1.80	0.64	0.27
										Sarapiqui													
BT-020406-2	299.71	19.14	45.43	1.62	231.12	5.06	11.44	1.88	9.60	2.76	0.93	3.00	0.46	3.10	0.60	1.84	1.87	0.27	1.28	0.09	1.32	0.38	0.12
IN-020506-1	272.78	24.99	69.33	2.90	365.48	8.30	17.86	2.85	13.82	3.74	1.18	3.96	0.61	4.03	0.76	2.34	2.35	0.36	1.85	0.17	1.49	0.70	0.22
IN-020506-2	258.14	30.26	70.52	2.88	322.48	7.86	16.96	2.72	13.44	3.68	1.14	3.93	0.60	3.94	0.79	2.45	2.42	0.37	1.90	0.17	1.52	0.76	0.33
IN-020506-3	279.96	25.77	69.94	2.95	369.89	8.78	18.97	3.00	14.45	3.85	1.22	4.16	0.64	4.07	0.78	2.43	2.42	0.38	1.86	0.16	1.54	0.71	0.24
IN-020506-4	283.62	28.46	76.69	2.76	418.93	8.71	18.07	2.88	14.12	3.93	1.28	4.17	0.66	4.31	0.86	2.68	2.76	0.43	1.97	0.16	2.21	0.78	0.26
IN-020506-5	293.59	26.06	61.48	2.19	255.42	7.87	17.01	2.80	13.72	3.70	1.18	4.00	0.63	4.16	0.81	2.51	2.59	0.40	1.70	0.12	1.28	0.54	0.14
IN-020506-6	312.40	26.61	66.45	2.39	273.89	8.30	17.83	2.97	14.53	3.86	1.22	4.13	0.65	4.25	0.83	2.59	2.60	0.39	1.84	0.13	1.42	0.59	0.18
IN-020506-7	309.91	26.66	68.57	2.44	286.66	8.72	18.85	3.11	15.11	3.97	1.26	4.31	0.65	4.35	0.84	2.64	2.65	0.39	1.81	0.13	1.29	0.58	0.27
IN-020806-1	228.29	24.58	72.00	2.82	378.05	8.66	18.45	2.97	13.43	3.80	1.16	3.93	0.64	3.85	0.75	2.23	2.36	0.37	2.11	0.20	1.55	0.82	0.41
IN-020806-2	206.86	15.35	37.23	2.23	203.45	4.31	10.14	1.55	7.85	2.18	0.80	2.41	0.36	2.39	0.46	1.46	1.44	0.22	1.11	0.17	1.62	0.41	0.18
IN-020806-3	249.02	19.80	61.00	4.76	223.87	6.85	14.42	2.14	10.26	2.69	0.98	2.99	0.48	3.03	0.61	1.79	1.83	0.28	1.47	0.27	1.10	0.41	0.18
IN-020806-4	319.44	28.17	92.77	6.04	325.03	9.25	19.81	3.10	15.00	4.04	1.36	4.29	0.69	4.41	0.87	2.69	2.73	0.42	2.25	0.36	1.74	0.57	0.18
IN-020806-5	171.77	13.67	33.69	1.22	180.38	3.97	8.97	1.39	7.07	2.06	0.68	2.19	0.32	2.27	0.41	1.25	1.28	0.19	0.89	0.06	0.87	0.27	0.10
PS-020706-1	267.88	23.79	55.45	1.71	313.82	6.28	13.78	2.30	11.50	3.28	1.09	3.66	0.57	3.71	0.72	2.28	2.22	0.35	1.53	0.10	1.40	0.48	0.16
PS-020706-2	220.03	22.73	77.98	4.48	419.39	7.71	17.11	2.54	12.01	3.24	1.09	3.44	0.55	3.57	0.69	2.23	2.31	0.35	2.04	0.27	1.90	0.79	0.23
AR-020206-1	311.39	22.92	-	2.11	298.16	7.21	15.22	2.37	11.63	3.09	1.12	3.34	0.54	3.49	0.69	2.09	2.25	0.34	1.35	0.12	1.46	0.53	0.29
AR-020206-2	291.02	24.12	55.45	2.04	300.08	6.96	15.30	2.48	12.17	3.34	1.15	3.62	0.57	3.66	0.71	2.28	2.30	0.36	1.47	0.11	1.29	0.59	0.29
AR-020206-3	297.66	28.33	63.02	2.75	333.10	7.42	15.96	2.58	12.45	3.49	1.14	3.91	0.61	4.16	0.86	2.70	2.89	0.47	1.71	0.16	1.89	0.72	0.20
AR-020206-4	350.81	20.79	47.39	1.82	205.09	5.65	12.46	2.04	10.36	2.88	1.01	3.21	0.49	3.29	0.64	1.98	2.00	0.31	1.33	0.12	1.55	0.44	0.19
AR-020206-5	316.42	24.25	54.87	2.15	262.15	6.26	13.51	2.23	11.18	3.14	1.06	3.41	0.53	3.68	0.71	2.27	2.26	0.34	1.46	0.12	1.38	0.40	0.20
AR-020206-6	194.65	29.87	73.79	2.81	349.87	9.07	19.54	3.26	15.91	4.26	1.39	4.69	0.73	4.72	0.94	2.89	3.00	0.47	1.95	0.16	1.82	0.62	0.39
AR-020206-7	152.32	29.24	79.75	3.71	386.43	9.70	20.84	3.45	16.61	4.39	1.44	4.73	0.73	4.66	0.91	3.00	3.02	0.46	2.09	0.23	2.59	0.71	0.39
AR-020206-8	223.76	27.49	123.88	3.84	470.59	11.68	24.52	3.80	17.11	4.24	1.14	4.38	0.70	4.26	0.82	2.61	2.65	0.41	3.11	0.25	2.83	1.68	0.74
CH-020406-1	229.53	25.61	96.37	3.65	462.38	10.48	21.94	3.37	16.13	4.45	1.31	4.17	0.65	4.10	0.79	2.42	2.50	0.38	2.45	0.22	2.23	1.07	0.47
CH-020406-2	229.85	27.00	81.46	2.90	395.35	9.26	19.45	3.06	14.31	3.71	1.19	4.03	0.61	4.06	0.78	2.45	2.50	0.39	2.07	0.17	1.63	0.85	0.39
CH-020406-4	228.46	25.51	94.63	3.37	410.31	9.80	20.87	3.25	15.14	3.95	1.17	4.13	0.64	4.07	0.78	2.41	2.48	0.37	2.39	0.20	2.15	1.05	0.38
CH-020406-5	150.01	26.02	126.79	4.67	631.70	12.18	25.09	3.69	16.30	4.14	1.17	4.20	0.66	4.14	0.81	2.57	2.85	0.45	3.17	0.31	3.14	1.54	0.49
BT-020406-3	145.25	31.42	67.21	2.25	314.88	7.84	18.47	3.17	16.57	4.75	1.68	5.18	0.81	5.24	1.03	3.17	3.24	0.48	1.81	0.12	1.94	0.54	0.42
BT-020406-5	229.46	15.90	39.54	1.49	147.70	3.44	7.88	1.18	6.04	1.79	0.65	2.12	0.34	2.48	0.47	1.49	1.51	0.24	1.01	0.08	1.03	0.25	0.14
BT-020406-6	272.67	20.09	55.88	2.42	216.39	5.50	12.03	1.89	9.31	2.62	0.92	2.94	0.47	3.16	0.61	1.91	1.94	0.30	1.42	0.14	1.99	0.35	0.16
BT-020406-7	253.07	18.53	55.57	2.40	265.20	6.38	14.27	2.20	10.86	2.87	1.03	3.00	0.45	2.96	0.55	1.72	1.76	0.26	1.44	0.21	2.61	0.50	0.35
BT-020406-8	146.38	30.83	65.01	2.17	304.22	7.46	17.39	2.99	15.69	4.49	1.62	5.01	0.78	5.02	0.98	3.10	3.10	0.47	1.80	0.11	1.54	0.50	0.16
BT-020406-9	237.24	31.95	100.44	3.60	447.33	10.56	22.69	3.70	17.72	4.79	1.45	5.21	0.83	5.13	1.01	3.05	3.12	0.48	2.65	0.22	1.49	1.07	0.31
BT-020406-10	279.91	22.42	52.00	1.87	246.36	5.95	13.30	2.15	11.02	3.21	1.07	3.47	0.54	3.60	0.70	2.12	2.13	0.34	1.42	0.11	1.28	0.48	0.21

Table 2. (continued)

Sample	V	Y	Zr	Nb	Ba	La	Ce	Pr	Nd	Sm	Eu	Gd	Tb	Dy	Ho	Er	Yb	Lu	Hf	Ta	Pb	Th	U
									Talamanca														
TC-1	50.61	26.83	203.11	6.50	1560.60	14.52	31.22	4.38	17.55	4.07	0.68	4.13	0.67	4.28	0.90	2.67	3.02	0.47	5.32	0.36	7.51	4.85	2.43
TA-021206-3	247.62	20.67	28.00	1.29	255.38	5.92	12.76	2.10	10.23	2.98	1.06	3.15	0.52	3.32	0.67	2.02	2.01	0.31	1.15	0.03	1.11	0.42	0.32
TA-021206-4	295.39	14.04	17.00	0.71	297.47	4.20	8.90	1.45	7.15	2.14	0.79	2.27	0.39	2.42	0.48	1.46	1.37	0.19	0.71	0.02	0.89	0.34	0.18
EG-1	342.04	14.08	24.07	0.69	339.46	4.46	9.80	1.67	8.10	2.31	0.66	2.57	0.42	2.56	0.51	1.40	1.35	0.20	0.77	0.04	0.92	0.41	0.23
TA-021206-6	253.92	21.28	57.00	2.01	718.08	9.22	18.39	2.90	12.73	3.49	1.10	3.52	0.57	3.51	0.69	2.01	2.07	0.32	1.67	0.11	0.81	0.90	0.53
TC-2	265.89	17.74	34.63	1.36	391.84	5.42	12.42	1.99	9.51	2.62	0.95	2.97	0.48	3.09	0.64	1.82	1.82	0.27	1.08	0.08	1.42	0.53	0.30
TC-4	315.08	16.61	33.54	1.51	406.87	4.98	11.39	1.77	8.43	2.41	0.89	2.78	0.45	2.90	0.60	1.69	1.71	0.26	1.05	0.08	1.71	0.66	0.28
TC-9	323.10	29.71	94.22	6.08	1826.11	19.71	42.38	6.03	25.43	5.95	1.50	5.85	0.88	5.27	1.04	2.91	2.90	0.43	2.75	0.28	1.56	2.76	1.08
									Paso Real														
GE-021306-4	169.40	13.90	101.00	8.03	988.91	27.42	51.75	6.28	22.33	4.28	1.25	4.37	0.59	2.57	0.47	1.39	1.37	0.20	2.48	0.45	6.17	4.07	2.24
GE-021306-5	279.91	17.41	99.00	8.00	799.04	28.47	54.32	7.17	27.70	5.50	1.68	5.21	0.68	3.19	0.58	1.62	1.61	0.23	2.45	0.39	2.53	3.55	1.37
GE-021306-6	257.87	16.94	57.00	4.50	833.80	24.32	46.02	6.28	24.82	5.14	1.53	4.77	0.63	3.03	0.56	1.60	1.61	0.23	1.82	0.22	3.42	2.54	0.82
GE-021306-7	172.15	13.36	80.00	5.99	885.25	20.60	39.21	4.88	18.30	3.68	1.14	3.73	0.53	2.44	0.46	1.34	1.34	0.20	2.14	0.36	4.56	2.51	0.94
GE-021306-8	226.03	17.11	51.00	4.33	964.00	22.96	43.30	5.86	23.21	4.72	1.47	4.53	0.62	3.00	0.56	1.63	1.68	0.25	1.67	0.23	4.10	1.48	0.57
GE-021306-9	303.35	19.50	60.00	5.53	1090.65	37.47	70.83	9.76	39.24	7.73	2.28	6.96	0.84	3.79	0.66	1.76	1.77	0.25	2.22	0.26	4.51	3.91	1.17
GE-021306-10	258.06	17.07	37.00	3.29	706.64	17.82	34.40	4.81	19.71	4.33	1.38	4.12	0.57	3.04	0.56	1.63	1.67	0.25	1.39	0.16	2.41	1.44	0.50
									Dominical														
DO-021406-1	450.28	20.89	45.00	1.55	310.55	7.47	14.28	2.38	11.15	3.15	1.03	3.26	0.54	3.40	0.67	2.01	2.02	0.31	1.51	0.10	0.79	0.74	0.37
DO-021406-2	316.76	15.44	29.00	1.14	394.55	5.43	10.97	1.77	8.37	2.37	0.87	2.50	0.42	2.58	0.52	1.57	1.53	0.23	1.08	0.03	1.56	0.52	0.32
TC-10a	463.52	24.60	53.24	1.88	767.07	8.52	19.13	3.12	14.49	3.95	1.30	4.35	0.70	4.40	0.88	2.47	2.49	0.37	1.70	0.11	3.33	0.88	0.45
									Aguacate														
CA-021106-1	280.03	18.15	47.22	2.38	417.94	7.11	14.34	2.11	10.30	2.76	0.94	3.00	0.45	3.00	0.56	1.71	1.68	0.26	1.22	0.12	1.30	0.85	0.17
CA-021106-2	261.57	42.82	107.33	4.56	696.59	10.41	22.44	3.88	20.00	5.93	1.81	6.69	1.09	7.13	1.43	4.52	4.45	0.69	3.10	0.25	2.87	1.33	0.39
CA-021106-3	226.84	18.66	58.36	1.97	522.75	6.31	12.97	1.92	9.04	2.52	0.83	2.78	0.45	2.88	0.55	1.74	1.77	0.27	1.48	0.12	1.61	0.95	0.27
CA-021106-4	294.16	28.01	50.53	2.14	559.45	18.03	27.52	4.47	20.56	4.59	1.51	4.80	0.65	3.85	0.74	2.25	2.12	0.32	1.17	0.08	1.87	1.11	0.23
CA-021106-5	269.42	21.31	57.54	2.54	635.97	15.12	29.63	4.27	19.18	4.41	1.39	4.23	0.58	3.42	0.62	1.89	1.92	0.29	1.36	0.09	2.30	1.57	0.38
CA-021106-6	255.59	20.42	66.44	3.88	568.51	18.05	35.97	5.01	21.64	4.79	1.46	4.51	0.61	3.40	0.61	1.81	1.78	0.27	1.50	0.15	2.09	1.80	0.42
CA-021106-7	239.37	17.89	51.09	1.92	837.84	17.13	30.13	3.92	16.94	3.65	1.19	3.53	0.48	2.81	0.52	1.67	1.69	0.26	1.34	0.09	3.02	4.69	0.86
LG-040105-1	463.00	19.11	59.00	3.81	618.00	20.62	46.50	6.30	27.43	5.58	1.74	5.08	0.65	3.29	0.59	1.58	1.52	0.22	1.39	0.15	2.68	1.33	0.77
LG-040105-2	208.87	26.88	85.00	5.52	1113.69	23.17	46.61	6.52	28.96	6.06	1.90	5.62	0.77	4.80	0.75	2.35	2.17	0.36	1.81	0.18	2.65	2.99	1.18
LC-010405-3	300.40	17.22	61.00	4.22	590.73	27.38	52.09	6.46	27.21	5.25	1.55	4.83	0.60	3.36	0.49	1.38	1.38	0.17	1.38	0.17	2.09	5.42	1.38
ACZ	199.04	21.95	125.00	6.66	893.37	34.89	67.62	8.53	34.79	7.94	1.96	5.91	0.76	4.12	0.64	1.86	1.96	0.29	2.45	0.29	2.61	5.29	2.16
CLC-1	238.11	14.24	91.00	5.77	863.53	28.37	54.15	6.51	26.77	4.79	1.47	4.70	0.57	2.82	0.40	0.98	0.98	0.12	1.72	0.25	3.01	5.53	1.60
CC-1	284.41	18.72	132.00	6.49	1020.27	51.36	95.71	11.40	43.93	7.53	2.20	6.40	0.73	3.77	0.52	1.46	1.99	0.21	2.41	0.31	3.01	10.67	3.66
CC-2	260.35	19.56	128.00	6.69	1025.92	52.72	95.50	11.40	45.19	7.74	2.20	6.75	0.81	3.97	0.60	1.57	2.09	0.21	2.62	0.31	4.54	10.88	2.62
CA-1	198.00	22.22	126.00	6.65	876.33	34.03	66.27	8.43	35.41	6.45	1.98	5.90	0.77	4.07	0.65	1.79	1.88	0.30	2.58	0.30	2.76	5.46	1.69

Table 2. (continued)

Sample	V	Y	Zr	Nb	Ba	La	Ce	Pr	Nd	Sm	Eu	Gd	Tb	Dy	Ho	Er	Yb	Lu	Hf	Ta	Pb	Th	U
LC-1	294.01	20.70	104.00	5.91	654.70	40.52	79.61	10.07	41.72	7.88	2.30	6.97	0.85	4.27	0.63	1.53	1.75	0.22	1.75	0.22	2.61	4.93	1.53
FR-1	235.53	19.92	88.00	5.12	741.78	28.54	53.09	6.50	26.67	5.04	1.54	4.77	0.63	3.50	0.53	1.71	1.79	0.24	1.79	0.24	2.30	4.31	1.38
SM-1	155.92	23.66	164.00	8.54	1192.17	54.63	112.82	14.65	55.52	10.70	3.12	10.03	1.16	4.60	0.74	1.92	2.08	0.30	3.39	0.49	5.59	6.64	2.50
P-95	351.19	19.61	55.51	2.55	675.61	11.68	24.77	3.71	16.55	4.08	1.02	4.12	0.62	3.64	0.71	1.93	1.83	0.27	1.48	0.12	2.79	1.51	0.59
										Standards													
JB-1a	201.75	28.34	-	32.16	512.37	41.93	66.29	7.30	27.29	5.13	1.42	5.47	0.79	4.45	0.86	2.39	2.20	0.34	4.00	2.05	4.87	11.61	1.42
JB-1a	193.84	22.94	-	29.85	500.91	36.88	66.22	7.42	27.67	5.21	1.50	5.24	0.75	4.00	0.78	2.14	2.09	0.30	3.46	1.87	4.90	9.60	1.47
JB-1a	190.37	24.55	-	29.84	502.50	38.21	65.22	7.37	28.08	5.49	1.52	5.69	0.81	4.22	0.84	2.35	2.21	0.33	3.76	1.96	4.80	10.08	1.44
JB-1a	203.23	22.00	-	26.94	507.39	38.62	66.89	6.86	23.72	4.87	1.44	5.48	0.75	3.82	0.69	2.05	2.14	0.17	3.11	1.65	6.38	8.43	1.35
JB-1a	195.00	22.88	-	26.98	508.39	38.32	66.69	7.44	25.48	5.09	1.47	5.51	0.78	3.93	0.72	2.06	2.12	0.32	3.26	1.77	6.12	8.94	1.40
JB-1a	194.28	23.10	-	26.77	500.23	38.23	66.10	7.42	25.54	5.12	1.49	5.51	0.79	3.95	0.73	2.09	2.14	0.32	3.26	1.79	6.25	9.03	1.41
JB-1a	194.84	23.13	-	26.76	501.13	38.72	66.48	7.49	25.86	5.09	1.48	5.63	0.79	3.87	0.72	2.13	2.19	0.32	3.30	1.79	6.37	9.14	1.43
JB-1a	190.20	23.64	-	26.63	501.92	38.71	65.87	7.43	25.39	5.05	1.50	5.57	0.81	4.00	0.76	2.15	2.13	0.32	3.25	1.74	6.18	8.99	1.36
JB-1a	189.46	23.69	-	26.84	495.26	38.55	65.62	7.43	25.72	5.04	1.48	5.51	0.79	4.06	0.76	2.17	2.18	0.34	3.32	1.80	6.15	9.05	1.34

time in Costa Rica and along the volcanic front from central Costa Rica to Nicaragua. We then explain these geochemical and petrological changes to be related to arc–hot spot interaction. To make quantitative estimation of our geological model of arc–hot spot interaction, we use Pb isotope systematics to define the percentage of contribution of the subducting Galapagos hot spot tracks. On the basis of the Pb isotopic sytematics, we model the entire suite of incompatible trace elements presented here and reported in the literature [*Carr et al.*, 2007] using significant input from subducting Cocos Plate sediments and contributions from the subduction Galapagos hot spot tracks off Costa Rica.

4.1. Temporal Magmatic Evolution in Costa Rica

[20] As mentioned in section 3, the Late Miocene to Pliocene lavas are mineralogically, petrologically, and geochemically distinct from the Oligocene through Middle Miocene lavas. The appearance of orthopyroxene as a phenocryst phase in the Late Miocene-Pliocene lavas could be the result of increasing silica content of the magmas via fractionation or by a metasomatic addition to the mantle source by silica-rich melts (melt-rock reaction) [e.g., *Kelemen et al.*, 1992]. Orthopyroxene-rich mantle peridotites from subduction zones are too high in SiO_2 and depleted in Al_2O_3 to be considered residues. Therefore, they are interpreted to be produced by the reaction of the mantle with melts from the subduction zone [*Herzberg*, 2004]. Melting of this metasomatized source will produce lavas that can crystallize orthopyroxene at the initial stages of crystallization; orthopyroxene bearing basaltic lavas are common in central Costa Rica since the Late Miocene. It is likely that the appearance of this mineral reflects a change in the source by metasomatic addition of silicate-rich melts to the mantle source. On the basis of the trace element compositions of volcanic rocks and olivine-hosted melt inclusions, recent studies have also argued that a component with melt-like characteristics (e.g., with low Ba/La but high La/Yb, La/Nb and probably also Cl, S, and F) controls many of geochemical peculiarities of the Costa Rican magmas [*Sadofsky et al.*, 2008].

[21] The change in geochemical character between the Oligocene-Middle Miocene and the Late Miocene-Quaternary volcanic rocks is also evident in major (Figure 4) and trace elements (Figure 5). The magmas change from low-K calc-alkaline series

Table 3. Radiogenic Isotopes Ratios Results[a]

Sample	87/86Sr	2σ	143/144Nd	2σ	$87/86S_{in}$	$143/144Nd_{in}$	206/204Pb	2σ	207/204Pb	2σ	208/204Pb	2σ	$206/204Pb_{in}$	$207/204Pb_{in}$	$208/204P_{in}$
							Trinidad								
P-125	0.703534	0.000005	0.513012	0.000006	**0.703501**	**0.512981**	18.677	0.002	15.562	0.002	38.364	0.005	**18.634**	**15.560**	**38.330**
P-126*	0.703540	0.000002	0.513020	0.000002	**0.703507**	**0.512989**	18.692	0.001	15.554	0.001	38.354	0.003	**18.649**	**15.552**	**38.320**
P-127*	0.703636	0.000002	0.513007	0.000003	**0.703604**	**0.512976**	18.730	0.002	15.587	0.002	38.486	0.004	**18.688**	**15.585**	**38.453**
							Sarapiqui								
BT-020406-2	0.703618	0.000008	0.513018	0.000008	**0.703601**	**0.513018**	18.616	0.001	15.516	0.001	38.221	0.003	**18.596**	**15.515**	**38.200**
IN-020506-2	0.703589	0.000006	-	-	**0.703552**	-	18.662	0.006	15.514	0.005	38.253	0.011	**18.614**	**15.512**	**38.217**
IN-020506-6	0.703585	0.000008	0.512990	0.000008	**0.703557**	**0.512967**	18.615	0.006	15.509	0.005	38.235	0.012	**18.587**	**15.508**	**38.205**
PS-020706-1	0.703723	0.000008	-	0.000016	**0.703711**	-	18.645	0.004	15.535	0.004	38.288	0.008	**18.620**	**15.534**	**38.263**
IN-020806-1	0.703775	0.000011	-	-	**0.703724**	-	18.650	0.007	15.526	0.006	38.280	0.014	**18.592**	**15.523**	**38.242**
AR-020206-2	0.703613	0.000011	0.513021	0.000008	**0.703597**	**0.513003**	18.619	0.011	15.562	0.010	38.285	0.025	**18.581**	**15.560**	**38.259**
AR-020206-3	0.703584	0.000025	0.513030	0.000003	**0.703563**	**0.513011**	18.621	0.002	15.528	0.002	38.234	0.004	**18.603**	**15.527**	**38.212**
AR-020206-4	0.703533	0.000006	0.513059	0.000025	**0.703519**	**0.513040**	18.576	0.005	15.536	0.004	38.230	0.010	**18.555**	**15.535**	**38.214**
AR-020206-6	0.703603	0.000007	0.513022	0.000002	**0.703580**	**0.513004**	18.580	0.003	15.530	0.002	38.211	0.006	**18.544**	**15.528**	**38.192**
AR-020206-7	0.703590	0.000007	0.513011	0.000006	**0.703563**	**0.512993**	18.635	0.009	15.556	0.007	38.300	0.019	**18.609**	**15.555**	**38.285**
CH-020406-2	0.703589	0.000008	-	-	**0.703569**	-	18.642	0.004	15.526	0.003	38.227	0.008	**18.606**	**15.524**	**38.201**
CH-020406-5	0.703751	0.000007	0.513020	0.000008	**0.703701**	**0.513005**	18.704	0.002	15.554	0.002	38.377	0.005	**18.680**	**15.553**	**38.352**
							Talamanca								
TA-021206-4	0.703843	0.000008	0.512996	0.000016	**0.703838**	**0.512998**	18.655	0.010	15.503	0.008	38.238	0.020	**18.627**	**15.502**	**38.220**
TC-1**	0.704269	0.000003	0.513022	0.000002	**0.704162**	**0.513022**	18.730	0.000	15.538	0.000	38.357	0.001	**18.692**	**15.536**	**38.332**
TC-2**	0.703864	0.000003	0.512997	0.000002	**0.703856**	**0.512997**	18.628	0.001	15.538	0.001	38.282	0.003	**18.599**	**15.537**	**38.265**
TC-4**	0.703749	0.000003	0.512995	0.000002	**0.703744**	**0.512995**	18.822	0.001	15.550	0.001	38.492	0.002	**18.800**	**15.549**	**38.475**
TC-9**	0.704031	0.000003	0.512993	0.000002	**0.704008**	**0.512993**	18.819	0.001	15.542	0.001	38.447	0.001	**18.739**	**15.539**	**38.380**
EG-1**	0.703844	0.000003	0.512974	0.000019	**0.703839**	**0.512975**	18.658	0.004	15.530	0.003	38.263	0.007	**18.624**	**15.528**	**38.243**
							Paso Real								
GE-021306-4	0.703780	0.000008	0.512980	0.000017	**0.703775**	**0.512977**	19.111	0.002	15.575	0.001	38.809	0.003	**19.098**	**15.575**	**38.801**
GE-021306-8	0.703737	0.000006	0.512986	0.000006	**0.703734**	**0.512983**	18.961	0.014	15.519	0.010	38.653	0.022	**18.956**	**15.519**	**38.649**
GE-021306-9	0.703512	0.000006	0.512967	0.000017	**0.703511**	**0.512964**	19.039	0.009	15.574	0.007	38.775	0.018	**19.030**	**15.574**	**38.765**
							Dominical								
TC-10a	0.704565	0.000003	0.513025	0.000003	**0.704518**	**0.513006**	18.638	0.001	15.548	0.001	38.309	0.002	**18.614**	**15.547**	**38.293**
							Aguacate								
CA-021106-1	0.703711	0.000009	0.513019	0.000042	**0.703708**	**0.513008**	18.772	0.004	15.540	0.003	38.418	0.008	**18.758**	**15.539**	**38.395**
CA-021106-2	0.703763	0.000006	0.513021	0.000030	**0.703747**	**0.513008**	18.702	0.005	15.532	0.003	38.308	0.007	**18.687**	**15.531**	**38.291**
CA-021106-4	0.703783	0.000008	-	-	**0.703776**	-	18.699	0.003	15.527	0.003	38.346	0.007	**18.693**	**15.527**	**38.336**

Table 3. (continued)

Sample	87/86Sr	2σ	143/144Nd	2σ	87/86S_{in}	143/144Nd_{in}	206/204Pb	2σ	207/204Pb	2σ	208/204Pb	2σ	206/204Pb_{in}	207/204Pb_{in}	208/204P_{in}
CA-021106-5	0.703914	0.000008	0.512956	0.000023	**0.703911**	**0.512951**	18.869	0.015	15.527	0.012	38.553	0.030	**18.861**	**15.527**	**38.541**
CA-021106-6	0.703947	0.000008	0.513000	0.000005	**0.703943**	**0.512996**	18.926	0.001	15.547	0.001	38.643	0.003	**18.916**	**15.547**	**38.629**
CA-021106-7	0.703868	0.000007	0.512971	0.000007	**0.703866**	**0.512968**	18.914	0.001	15.537	0.001	38.603	0.002	**18.903**	**15.536**	**38.583**
CA-021106-8	-	-	-	-	-	-	19.096	0.001	15.573	0.001	38.837	0.003	**19.085**	**15.573**	**38.817**
LG-040105-1	0.704045	0.000007	0.512991	0.000024	**0.704040**	**0.512986**	-	-	-	-	-	-	-	-	-
CC-2	0.703817	0.000007	0.512982	0.000006	**0.703811**	**0.512979**	19.136	0.006	15.572	0.004	38.890	0.011	**19.113**	**15.571**	**38.858**
LC-1	0.703922	0.000006	0.512986	0.000005	**0.703913**	**0.512959**	18.949	0.009	15.536	0.007	38.677	0.019	**18.911**	**15.534**	**38.637**
P-95	0.703752	0.000007	0.512991	0.000004	**0.703743**	**0.512985**	18.873	0.001	15.557	0.001	38.575	0.002	**18.860**	**15.556**	**38.564**

[a] Age corrected ratios (in) in bold. Asterisk indicates Pb, Sr and Nd concentrations for age-correction assumed the same as sample from sample P-125. Two asterisks indicate data from *Hoernle et al.* [2008]. The initial ratios were calculated with the average ages reported in the literature or in this study (Table 1) for each geologic unit.

during the Oligocene-Middle Miocene, to high-K calc-alkaline to transitional shoshonitic series in the Late Miocene-Quaternary volcanic rocks (Figure 4). Primitive mantle-normalized trace element patterns (Figure 5) reveal slightly lower Y and heavy REE abundances in the Late Miocene to Quaternary central Costa Rican volcanic front lavas compared to the Oligocene-Middle Miocene samples. The lower Y and heavy REE abundances are possibly due to greater amounts of garnet in the residue (subduction oceanic cust and/or veins of garnet pyroxenite) as suggested by *Feigenson and Carr* [1986]. For elements to the left of Ti in Figure 5, the Oligocene-Middle Miocene samples show patterns that mimic the modern Nicaraguan volcanic front lavas, with the exception of some of the fluid mobile elements Ba, U, and Pb (Figure 5). The higher values for these fluid mobile elements in the modern Nicaraguan arc can be explained by the subduction of different sediments over time, as suggested by *Patino et al.* [2000] and *Plank et al.* [2002]. It is also worth noting that the Sr isotope ratio begins decreasing after the "carbonate crash," believed to have been caused by an ~800 m rise in the carbonate compensation depth as the Central American isthmus gateway began to close around 10 Ma ago [*Plank et al.*, 2002]. The addition of hemipelagic sediments to the sediment column may have reduced the concentration of Sr in the overall sediment pile. Compared to the older Costa Rica samples and the modern Nicaraguan volcanic front lavas, Central Costa Rican samples younger than 6 Ma are strongly enriched in most incompatible elements, including fluid (e.g., Ba, K, Sr, K, etc.) and melt (e.g., Nb, Ta, Ce, Nd, Zr, etc.) mobile incompatible elements.

[22] The temporal evolution of the key geochemical parameters (Pb, Nd, Sr isotopes and La/Yb) were summarized above and are shown in Figure 6. The Galapagos-OIB signature in Costa Rica volcanic-front rocks is characterized by $^{206}Pb/^{204}Pb \geq 18.9$, $^{208}Pb/^{204}Pb > 38.5$, $^{143}Nd/^{144}Nd \leq 0.51298$, and La/Yb > 10 (Figure 6). This signature is first evident in the Late Miocene (~6 Ma) samples. The Oligocene-Middle Miocene samples have $^{206}Pb/^{204}Pb < 18.8$, $^{208}Pb/^{204}Pb < 38.4$, $^{143}Nd/^{144}Nd > 0.51297$, and La/Yb < 6 values, typical of normal arc volcanic rocks and close to the Nicaraguan volcanic front lavas (Figure 6). The appearance of the Galapagos-OIB signature in central Costa Rica at ~6 Ma correlates with the eruption of alkaline basalts in the back-arc and adakites in southern Costa Rica and Panama. The isotopic and trace element ratios of the alkaline

Table 4. Summary of the Different Models Shown in Figure 10[a]

Segment	Galapagos Hot Spot Contribution	Sediment Component	Degree of Melting	Garnet in the Source
Central Costa Rica	3.0%	0.1%	8%	1.5%
NW Costa Rica	0.6%	0.6%	9%	0.5%
SE Nicaragua	0.4%	0.4%	6%	0.3%
NW Nicaragua	-	0.6%	8%	0.3%
Late Miocene-Pliocene	0.5%	0.6%	4%	1.0%
Oligocene-Mid. Miocene	-	0.6%	8%	0.3%

[a] The Galapagos contribution and sediment refer to the metasomatic additions to a DM mantle from melts the subducting slab. Notice that the degree of partial meting used in each model is in the same order of magnitude and does not change significantly along the volcanic front. The modal garnet needed to fit the heavy REE patterns only occurs along with the metasomatic contribution of the Galapagos hot spot.

basalts and adakites overlap with and extend to even higher La/Yb and Pb isotope ratios and lower Nd isotope ratios than the Costa Rican volcanic front lavas (Figure 6). This geochemical change coincides in central Costa Rica with a tectonic discordance reported by *Denyer and Arias* [1991] between the La Cruz Formation (11.35–10.90 Ma) [*MacMillan et al.*, 2004] and the Grifo Alto Formation (5.10–4.04 Ma) [*Marshall et al.*, 2003; *MacMillan et al.*, 2004]. Samples from the Grifo Alto Formation have the enriched isotopic ratios and trace element values representative of the modern Galapagos-OIB signature in central Costa Rica (Figures 5 and 6).

4.2. Geochemical Components of the Southern Central American Lavas

[23] The subducting crust on the incoming plates outboard of Nicaragua, Costa Rica, and Panama is geochemically heterogeneous (Figure 1). The crust in front of Nicaragua was formed at the East Pacific Rise-Cocos spreading center and has a normal MORB-type geochemical composition [*Werner et al.*, 2003] (Figure 7). The subducting crust in front of central Costa Rica and Panama is covered by Galapagos hot spot tracks that preserve the geochemical zonation of the Galapagos hot spot domains [*Hoernle et al.*, 2000; *Werner et al.*, 2003]. The subducting Seamount Province in front of central Costa Rica includes a series of small seamounts and submerged oceanic islands. These Seamount Province lavas show an OIB-alkaline composition and an isotopic signature belonging to the Northern Galapagos Domain [*Hoernle et al.*, 2000; *Werner et al.*, 2003, *Harpp et al.*, 2004] (Figure 1). The subducting Cocos and Coiba ridges have an OIB-tholeiitic composition and are more isotopically heterogeneous (Central, Eastern, and Southern Galapagos domains). However, the dominant isotopic domain in these ridges is the Central Galapagos Domain [*Hoernle et al.*, 2000; *Werner et al.*, 2003] (Figure 1).

[24] The B, Be, and Th isotope systematics of the volcanic front lavas require the contribution of the subducted sediments [*Leeman et al.*, 1994; *Reagan et al.*, 1994]. Similarly, the Sr isotopes are controlled by melts and/or hydrous fluids from the subducting sedimentary section of the Cocos Plate [*Patino et al.*, 2000] and fluids from the subducting oceanic crust and deserpentinization of the subducting mantle [*Ranero et al.*, 2003]. Nd isotope systematics in Central America are more complicated. In Nicaragua, *Carr et al.* [1990] modeled the volcanic front lavas as a mix of a DM component and a small amount of sediment. However, this mix does not provide sufficient Nd to explain the Nd concentrations of the erupted lavas, thus some Nd is required from the subducting oceanic crust [*Patino et al.*, 2000, and this study].

[25] In contrast to other isotopic systems, Pb isotope systematics show no convincing evidence for contribution of subducted sediments [*Hoernle et al.*, 2008]. This may be due to decoupling between highly fluid-mobile Pb flushed at shallower levels (fore-arc vents?) and the relatively fluid-immobile Be, Th, and Nd possibly released at deeper levels. Alternatively, the integrated slab fluid that reacts with the mantle wedge does not shift the Pb isotope composition of the mixture because the subducting sediments are close to the composition of DM [*Feigenson et al.*, 2004]. Therefore, Pb isotope systematics in southern Central America are mostly controlled by the interaction between the subducting oceanic crust and DM [*Hoernle et al.*, 2008, Figure 7].

[26] In summary the Pb isotope systematics of the data presented here (Figure 7) are explained by three main components. The first is an unradiogenic component that could either be normal

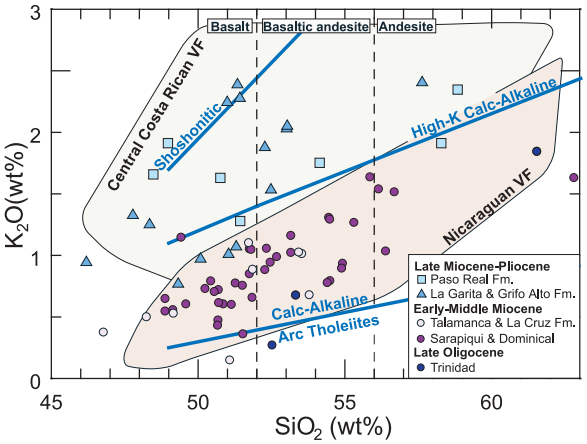

Figure 4. Geochemical classification for the Oligocene to Pliocene samples. Note that most the Upper Miocene-Pliocene samples are higher in K_2O at a given SiO_2, generally having high-K calc-clkaline to shoshonitic compostions similar to the Costa Rican volcanic front. Most Oligocene-Middle Miocene samples have calc-alkaline compositions similar to Quaternary Nicaragua lavas. Fields for the modern volcanic fronts of central Costa Rica (gray) and Nicaragua (light red) are from *Carr et al.* [2003]. All samples normalized on a volatile free basis.

subducting Cocos/Nazca oceanic crust or depleted mantle (DM) in the wedge. The other two components are highly radiogenic and derived from the Galapagos hot spot. These two radiogenic components are the subducting Seamount Province (Northern Galapagos Domain) and the subducting Cocos/Coiba Ridge (Central Galapagos Domain) (Figure 7). Nd isotopes require the aforementioned components as well as an input from subducting sediments (Figure 7). Most of the isotopic ratios of the samples >10 Ma can be explained by the interaction of normal oceanic crust or DM and subducted sediments (for Nd isotopes), analogous to those from the Nicaraguan volcanic front lavas. The samples from the Upper Miocene-Pliocene units (La Garita Fm., Grifo Alto Fm., and Paso Real Fm., $^{206}Pb/^{204}Pb$ > 18.8; Figure 7) trend toward a composition intermediate between the Cocos/Coiba Ridge and the Seamount Province components. This intermediate composition suggests that mixing between the two Galapagos components occurred in the mantle wedge (section 4.3). The data from the modern central Costa Rica volcanic front and the alkaline basalts require a Seamount Province component whereas adakites and alkaline lavas from southern Costa Rica and Panama are in range with the Cocos/Coiba Ridge component [*Hoernle et al.*, 2008].

4.3. Arc–Hot Spot Interaction

[27] The interaction between a subduction system and a hot spot can occur in at least two different tectonic scenarios. An enriched mantle plume could flow into the wedge of a subduction zone if the arc passes over or is merely close to it. A different interaction can occur when the eruptive products of a plume (e.g., seamount tracks or aseismic ridges), subduct beneath an arc. Subduction of hot spot tracks can "refertilize" the arc

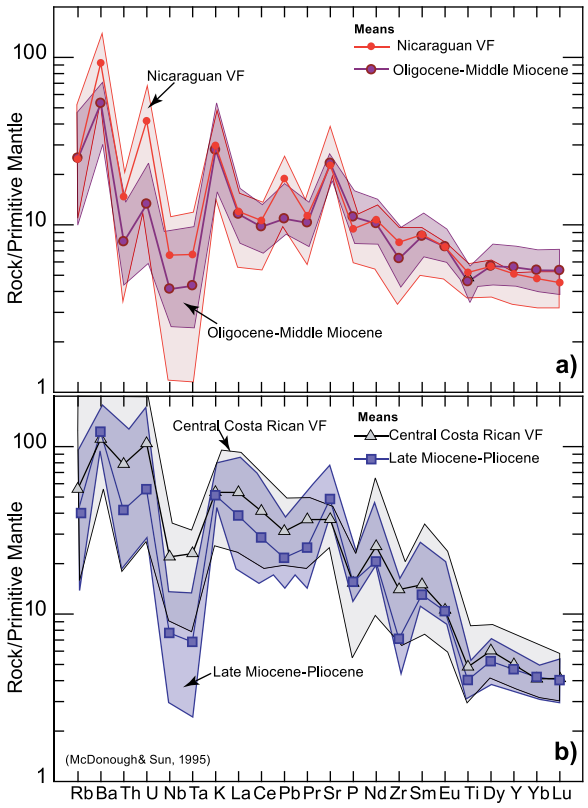

Figure 5. Primitive-mantle normalized diagram of the (a) Oligocene-Middle Miocene and (b) Late Miocene-Pliocene samples, compared to incompatible-element patterns of the volcanic fronts of Nicaragua and central Costa Rica [*Carr et al.*, 2003, 2007]. The Oligocene-Middle-Miocene and Late Miocene-Pliocene sample means include lavas with SiO_2 < 63 wt% reported in Tables 1 and 2. Note that the Oligocene-Middle Miocene samples from Costa Rica have patterns similar to the modern Nicaraguan volcanic front lavas and are relatively depleted compared to modern central Costa Rican lavas. The Late Miocene-Pliocene samples have patterns similar to the central Costa Rican volcanic front (VF) lavas.

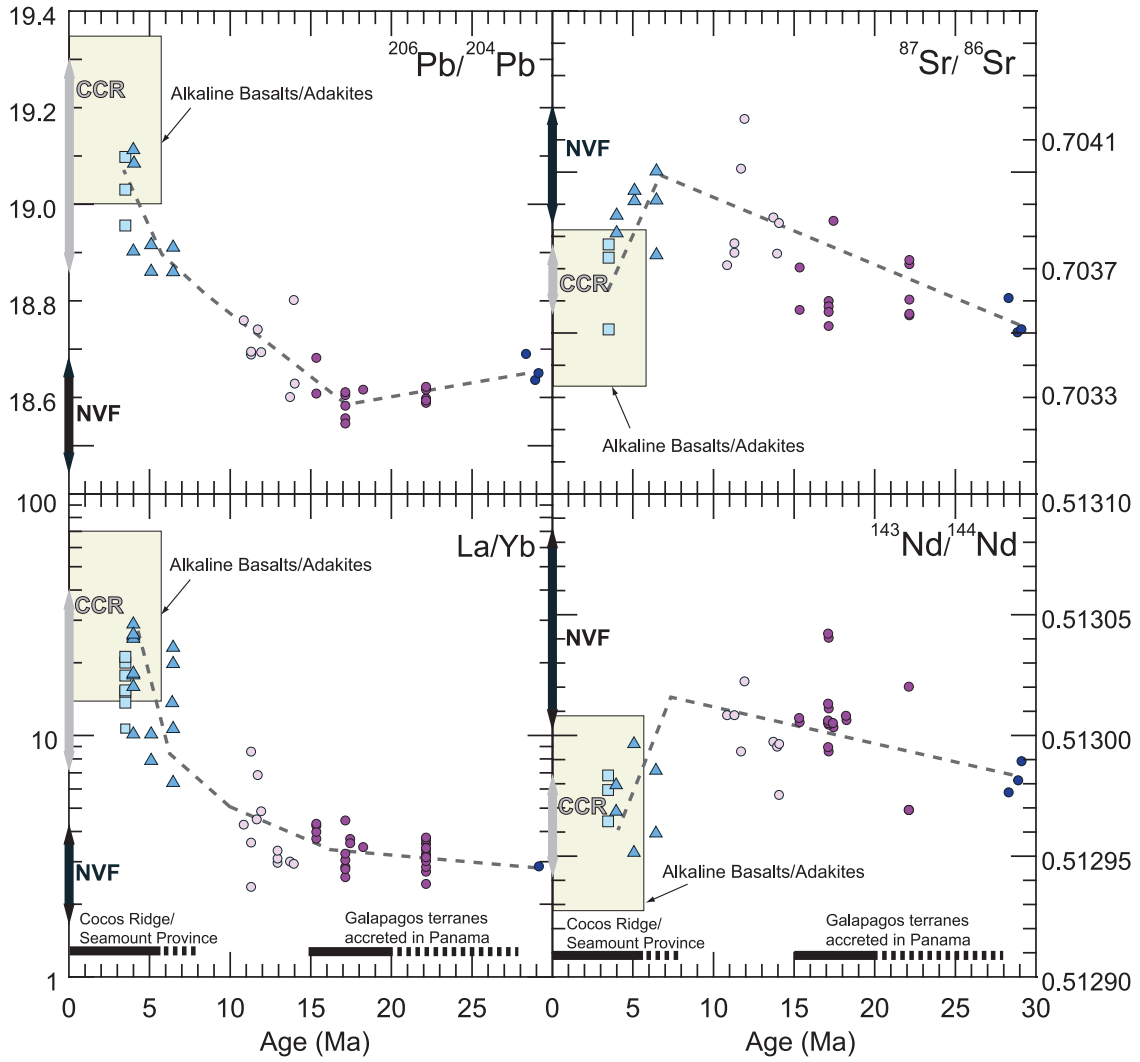

Figure 6. La/Yb and age-corrected Pb, Sr, and Nd isotopic ratios of Oligocene to Pliocene arc-related volcanic rocks are plotted against age in Ma. The range for modern volcanic fronts of central Costa Rica (CCR) and Nicaragua (NVF) are shown on the *y* axis. The appearance of alkaline basalts from the central Costa Rica area and alkaline basalts and adakites from southern Costa Rica and Panama coincide with the appearance of the new source about ~6 Ma ago. The time frame for accretionary processes and the collision of the Cocos Ridge and Seamount Province is shown at the bottom on the *x* axis and discussed in the text. Data for the volcanic front, alkaline basalts and adakites are from *Hoernle et al.* [2008]. Ages of the Galapagos hot spot accreted terrains in Panamá are from *Hauff et al.* [2000] and *Hoernle et al.* [2002]. Symbols are the same as Figure 4.

mantle source by metasomatic processes (fluids and/or melts). Subsequent melting of this metasomatized mantle could produce lavas with an OIB signature.

[28] *Wendt et al.* [1997] reported Pb isotopes and trace element evidence for the interaction of the northern segment of the Tonga-Kermadec arc with two hot spot components. The Samoa mantle plume flows into the northern segment of the arc and the Louisville seamount chain subducts into the central part of the arc. In both cases the erupting lavas show an enriched geochemical signature. The OIB signature in alkaline lavas from the Mexican volcanic belt has been explained as a consequence of an arc–hot spot interaction involving plume activity below the arc [*Márquez et al.*, 1999]. *Bryant et al.* [2006] reported Pb, Sr, and Nd isotopic and trace element evidence for the interaction between melts from the Carnegie Ridge (Galapagos hot spot track) (Figure 1) and the mantle wedge in the northern Andean volcanic zone in Ecuador with minor continental crust assimilation. Independent of the nature of the

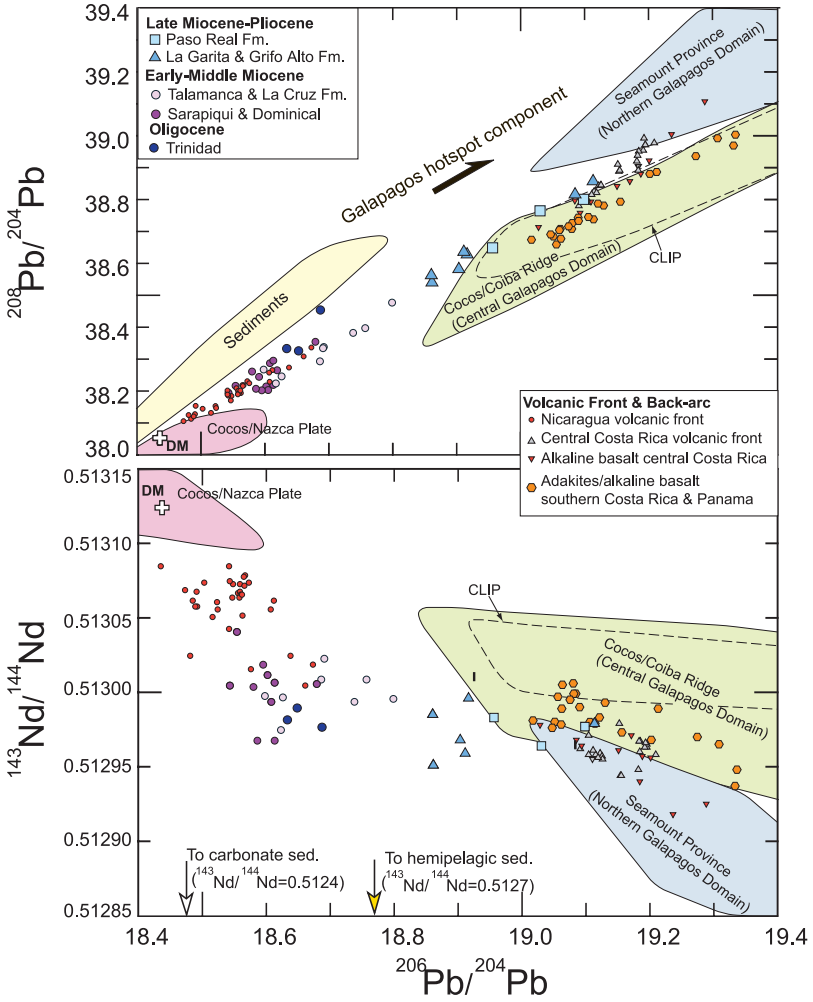

Figure 7. Age-corrected Pb and Nd isotopic ratios for samples and possible sources of the Oligocene-Pliocene samples, the central Costa Rican and Nicaraguan volcanic front lavas, and alkaline basalts and adakites from Costa Rica and Panama. Additional data for the Seamount Province, Cocos/Coiba Ridge, and Cocos/Nazca Plate are from *Hoernle et al.* [2000] and *Werner et al.* [2003]. The fore-arc CLIP oceanic complexes are from *Hauff et al.* [2000] and *Hoernle et al.* [2004], and subducting sediments are from *Feigenson et al.* [2004]. The volcanic front lavas and alkaline basalts from central Costa Rica require a subducting Seamount Province component (Northern Galapagos Domain, also see Figure 1). The alkaline basalts and adakites from southern Costa Rica and Panama are in range with the subducting Cocos/Coiba Ridge (Central Galapagos Domain, also see Figure 1). The modern Galapagos-OIB signature in central Costa Rica appears in the Late Miocene-Pliocene units (~6 Ma). Intermediate values ($^{206}Pb/^{204}Pb$ = 18.7–18.8) in the Oligocene-Middle Miocene samples possibly reflect the effect of the interaction of older Galapagos hot spot tracks with southern Central America.

interaction between an arc and a hot spot, the result will be arc lavas with an anomalous enriched geochemical signature.

[29] The present-day geographic distribution of the Galapagos signature in the volcanics of Costa Rica and Panama is onshore from the ongoing collision of Galapagos hot spot tracks with the Middle American Trench (Figure 1). In central Costa Rica, where the Seamount Province has been subducted (see projected lines and blue areas in Figure 1), the samples from the volcanic front and the back-arc alkaline lavas (Figure 1) require a Seamount Province (Northern Galapagos Domain) geochemical component (Figure 7), whereas the southern Costa Rica and Panama adakites and alkaline lavas are in the isotopic range of the Cocos/Coiba Ridge component (Central Galapagos Domain) (Figure 7). Geophysical studies reveal that not only the subducting tracks may interact with the southern Central American margin but also there may be interaction with the Galapagos hot spot plume material, since a low-velocity seismic anomaly is

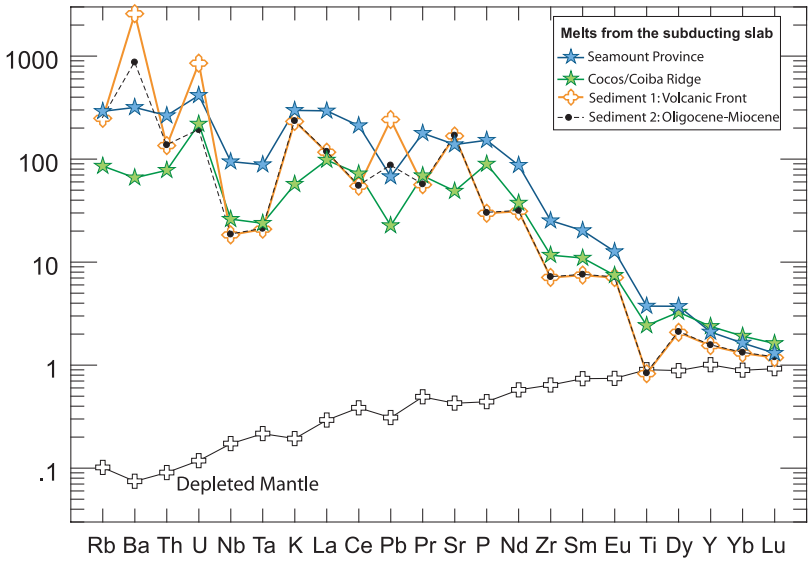

Figure 8. Trace element compositions of the different modeled components for this study (model data in Appendix A). DM was inverted with a melt fraction of 8% from the sample SO 144–1 [*Werner et al.*, 2003] with a modal composition of 60%olivine + 25% orthopyroxene + 13%clinopyroxene + 2%spinel. Melts from the mean subducting Cocos/Coiba Ridge and Seamount Province [*Hoernle et al.*, 2000; *Werner et al.*, 2003] were modeled with melt fraction of 20% with a modal composition of 83%clinopyroxene + 15%garnet + 2% rutile. Sediment melt 1 was modeled from a mix of a 70% mean hemipelagic + 30% mean carbonate from *Patino et al.* [2000]. The sediment melt 1 was modeled with melt fraction of 20% and a modal composition of 84.6% clinopyroxene + 15%garnet + 0.4rutile. There is no information about the subducting sediments during the Oligocene-Pliocene. Thus, sediment melt 1 composition was empirically adjusted (reducing Ba, U, and Pb) to fit the average value of the Oligocene-Pliocene samples.

detected up to southern Costa Rica margin [*Montelli et al.*, 2006]. However, the central Costa Rican volcanic front lavas show significant Nb, Ta, and Ti depletions typical of arc volcanism [e.g., *Carr et al.*, 2007], indicating that at least in the volcanic front the enriched Galapagos hot spot component went through the subduction process that separated those elements from the other incompatible elements and thus possibly represent a subduction input and not a mantle composition.

[30] The isotopic and trace element data described here indicate that the central Costa Rican Galapagos-OIB signature results from metasomatism of the mantle wedge by melts and/or fluids from the subducting Galapagos hot spot tracks. The intermediate Pb isotopic values ($^{206}Pb/^{204}Pb$ = 18.7–18.8; Figures 6 and 7) of some of the samples from the Middle Miocene might be explained as an input from the subduction of older Galapagos hot spot tracks that collided with southern Central America during the Miocene [*Hoernle et al.*, 2002].

[31] Estimates for the timing of the collision of the Cocos Ridge, the Seamount Province, and possibly older tracks with southern Central America range from 10 to 1 Ma [*Gardner et al.*, 1992; *Johnston and Thorkelson*, 1997; *Gräfe et al.*, 2002; *Silver et al.*, 2004; *MacMillan et al.*, 2004]. Our new data show that the Galapagos-OIB signature appears in central Costa Rica at ~6 Ma ago (sample P-95 from La Garita Formation). This particular geochemical signature allows us to constrain the initial collision of the Galapagos hot spot tracks at ~8 Ma, allowing ~2 Ma for the subducted tracks to move from the trench to a melt generating depth of ~100 km beneath the arc (using the current average convergence rate of 80 mm/a). This calculation agrees with the geophysical evidence of a major tectonic event in the Pacific coast of southern Costa Rica circa 8–10 Ma, possibly triggered by the collision of the margin with Galapagos hot spot tracks [*Silver et al.*, 2004] as with elevated subduction erosion rates beginning ~6 Ma ago [*Vannucchi et al.*, 2006].

[32] The southern Central American margin has been interacting with the Galapagos hot spot throughout its geologic history. This interaction began with the formation of the Caribbean Large Igneous Province (CLIP) (139–85 Ma [*Hoernle et al.*, 2000; *Denyer et al.*, 2006]). Subsequently, oceanic islands and aseismic ridges were accreted

during the Eocene and Miocene [*Hoernle et al.*, 2000; *Denyer et al.*, 2006]. The interaction continues with the relatively recent subduction of the hot spot tracks. The mantle wedge enrichment produced by the subduction of the hot spot tracks can be considered an important stage in the global cycle of oceanic crust recycling and mantle refertilization by metasomatic processes.

4.4. Isotopic and Trace Element Modeling of the Arc–Hot Spot Interaction in Southern Central America

[33] To evaluate the implications of our subduction–hot spot interaction model, we estimate the regional and temporal contribution of the Galapagos hot spot to magmatism in southern Central America. According to *Peacock et al.* [2005] the thermal properties of the subduction zone of Costa Rica and Nicaragua allow the subducting sediments and the uppermost part of subducting oceanic crust to partially melt. We consider melting of the subducting slab an important part of the metasomatic processes inferred from the previous discussion of the spatial and temporal geochemical changes in southern Central America.

[34] The melting model used in this study is aggregated fractional melting [*Shaw*, 1970] and the partition coefficients used in our modeling (peridotite and eclogite sources) are from the compilation of *Kelemen et al.* [2003]. The first modeling requirement is a mantle wedge with a DM composition that makes an appropriate isotopic and trace element end-member. We obtained a locally appropriate DM by inverting using a melt fraction of 8% the sample SO-144-1 (Figure 8) from the EPR-Cocos crust off Nicaragua [*Werner et al.*, 2003]. This DM is similar to the modal and trace element composition reported by *Workman and Hart* [2005]. The Galapagos hot spot contributions were modeled from the mean values of the subducting Seamount Province and the Cocos/Coiba Ridge reported by *Hoernle et al.* [2000] and *Werner et al.* [2003], using 20% melting in the eclogite facies (Figure 8). The final components are two sediment melts based on the sediment compositions of *Patino et al.* [2000] and a melt fraction of 20%. Pr and Ta, not included in the original data, were interpolated from adjacent elements normalized to *McDonough and Sun* [1995] values. Pr_N (Ce_N, Nd_N) for the hemipelagics, Pr_N (L_N, Nd_N) for the carbonates, and Ta_N($\sim Nb_N$) for both sediments. The first sediment melt consists of a mix of 30% mean carbonate and 70% mean hemipelagic sediments (Figure 8). Because we do not have the actual composition of the sediment subducting during Oligocene-Pliocene, we used the same composition as sediment melt 1; but with some adjustments to fit the trace element data of the average Oligocene-Pliocene values, specifically, lower Ba, U and Pb (Figure 8). All the modeled results and details, including melt modes and melt fractions are in Appendix A and plotted in Figures 8–10.

[35] To constrain the Pb isotopic contribution from the subducting Galapagos hot spot tracks, we plotted a three component diagram that shows the interaction of DM with melts from the subducting Seamount Province and the Cocos/Coiba Ridge (Figure 9). In Figure 9a, the Galapagos hot spot contribution decreases systematically along the volcanic front from central Costa Rica to NW Nicaragua. The samples from southern Costa Rica and Panama are close to the mixing line between the subducting Cocos/Coiba Ridge and DM (Figure 9a). Along the volcanic front of Costa Rica and Nicaragua, the Galapagos hot spot contribution is actually a mix between the highly enriched subducting Seamount Province and the volumetrically major Cocos/Coiba Ridge. There are two clusters of data in the central Costa Rica volcanic front and both require >1% of the Galapagos hot spot contribution. The less radiogenic cluster, represented by samples from Barva, Irazú, and Turrialba volcanoes requires a mix of 20% Seamount Province plus 80% Cocos/Coiba Ridge melts (Figure 9a). The second cluster includes samples from Poás and Platanar volcanoes, which are located directly above the subducting Seamount Province. This group requires a mix of 40% Seamount Province plus 60% Cocos/Coiba Ridge melts (Figure 9a). The Galapagos hot spot contribution decreases to 1–0.5% in NW Costa Rica, 0.5–0.1 in SE Nicaragua, and it is negligible in NW Nicaragua.

[36] A temporal change in the contribution from the Galapagos hot spot is shown in Figure 9b. For most of the Oligocene-Middle Miocene samples, the Galapagos hot spot contribution was minor. The Middle Miocene samples from the Talamanca Range (southern Costa Rica, Figure 1) require about 0.5% of Galapagos hot spot contribution, with a major participation of a component similar to the Cocos/Coiba Ridge (Figure 9b). In the Late Miocene-Pliocene samples, the Galapagos hot spot contribution ranges between 0.1 and 2% and must

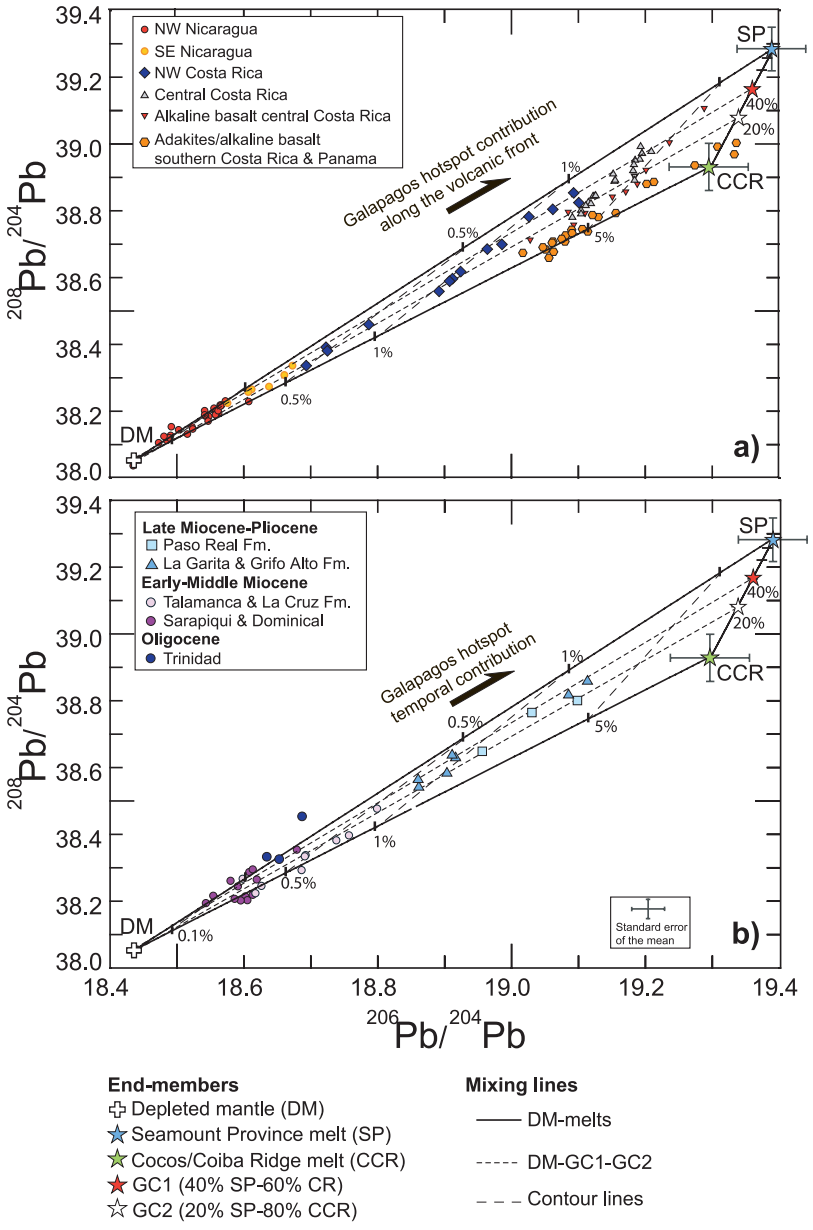

Figure 9. Mixing lines connect the modeled mean Seamount Province melt ($^{143}Nd/^{144}Nd = 0.51286$, $^{206}Pb/^{204}Pb = 19.390$, $^{208}Pb/^{204}Pb = 39.284$, N = 14) and the mean Cocos/Coiba Ridge melt ($^{143}Nd/^{144}Nd = 0.51297$, $^{206}Pb/^{204}Pb = 19.296$, $^{208}Pb/^{204}Pb = 38.930$, N = 17) [*Hoernle et al.*, 2000; *Werner et al.*, 2003] with the DM (inverted from sample SO 144–1) from *Werner et al.* [2003]. Notice that the Galapagos hot spot contribution decreases systematically (a) along the volcanic front and (b) in the older samples. The relative recent Galapagos OIB signature (with $^{206}Pb/^{204}Pb > 18.8$) appears in the Late Miocene-Pliocene samples (Figure 9b). The intermediate $^{206}Pb/^{204}Pb$ (18.7–18.8) from some of the Middle Miocene Talamanca Range (Figure 9b) could be explained by the interaction of the arc with older Galapagos hot spot tracks during the Miocene. The Galapagos hot spot participation is a mix between the volumetrically major Cocos Ridge and the less voluminous but highly enriched Seamount Province. GC1 is the Galapagos hot spot component for the volcanic front. It was modeled as 40% Seamount Province plus 60%Cocos/Coiba Ridge. GC2 is the Galapagos hot spot component for the Late Miocene-Pliocene units and was modeled as 20% Seamount Province plus 80% Cocos/Coiba Ridge.

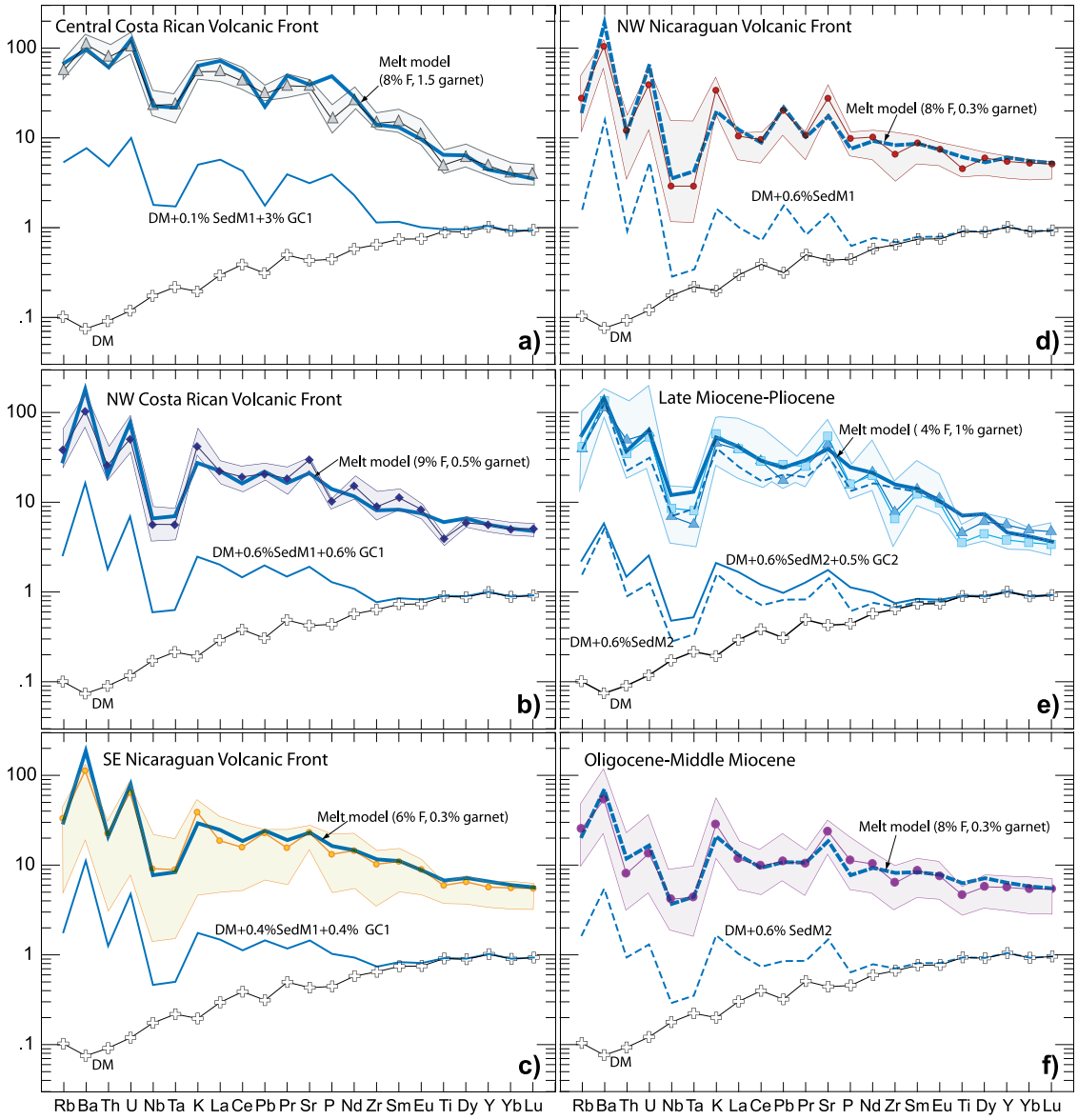

Figure 10. Trace element models compared with the mean (denoted by line with symbols) and range (denoted by shaded field enclosing the mean line) for each volcanic segment from Central Costa Rica to NW Nicaragua. The dashed blue lines show model melts derived from a DM mantle source metasomatized by melts from subducting sediments. Metasomatized mantle models that require a Galapagos hot spot component and liquids derived from that source are plotted as continuous blue lines. There is a good agreement between the models and the data. Misfits in P, Zr, and Ti could be explained by fractional crystallization at crustal levels. The Galapagos hot spot component was approximated from Figure 8 and represents a mix between melts of the Seamount Province (SP) and the Cocos/Coiba Ridge (CCR). GC1 is the Galapagos hot spot component for the volcanic front. It was modeled as 40% SPM plus 60%CCR. GC2 is the Galapagos hot spot component for the Late Miocene-Pliocene units and was modeled as 20% SP plus 80% CCR. SedM1, sediment melt 1; SedM2, sediment melt 2 (Oligocene-Miocene); F, melt fraction in percent.

be a mix between the Seamount Province component and the Cocos/Coiba Ridge component.

[37] To model the incompatible trace elements, we calculated average elemental concentrations of the main volcanic segments from central Costa Rica to NW Nicaragua, using the data from *Carr et al.* [2007] (Figure 10). We also calculated mean values of the Oligocene-Middle Miocene samples and Late Miocene-Pliocene samples to constrain the temporal effect of the interaction of the subduction zone with the Galapagos hot spot (Figure 10).

[38] The interaction between the subducting Galapagos hot spot tracks, the sediment and the DM mantle wedge is modeled as a three stage process. The first stage includes melting of the subducting crust (sediment and/or subducting oceanic crust) in eclogite facies. The second stage is visualized as a metasomatic melt-rock reaction between the melts from the slab and the mantle wedge in the garnet stability field and modeled as multicomponent mixing. The last stage is flux melting of this metasomatized or ''refertilized'' mantle caused by fluids from the subducting slab (slab dehydratation and/or subducting oceanic mantle deserpentinization) possibly in a shallower level but still in the garnet stability field. The modeled Galapagos hot spot contribution was based on the Pb isotopes in Figure 9. Small increments of sediment melt were added to the mantle until acceptable Rb, Ba, K, Pb, U, and Sr fits were obtained (within the modeled group range and close to the average calculation; Figure 10). According to *Thomsen and Schmidt* [2008] no more than 30% of the carbonates are recycled in the subarc mantle region. Therefore, we used sediment melt 1 (70% hemipelagic plus 30% carbonate) for the trace element modeling. However, the Nd isotopic systematics (Figure 7) and some of the trace element data from the volcanic front [*Patino et al.*, 2000] may require additional subducted carbonate. This component could be a hydrous fluid instead of a melt. The source modal composition after metasomatism is close to the original DM; however, a mass balance of clinopyroxene and garnet was required to fit the heavy REE data of each calculated mean in Figure 10.

[39] The different trace element models are plotted with the respective volcanic front segment means and temporal means in Figure 10. The most important observation of the trace element modeling is that the trace element concentrations observed along the arc, south of central Nicaragua require a Galapagos hot spot component. Trace element compositions in central Costa Rica lavas are explained by a DM metasomatized by 3% of the Galapagos hot spot contribution and <0.1% of sediment input, melted at 8% (Figure 10a). The trace element composition of NW Costa Rica require a DM metasomatized by about 0.6% of the Galapagos hot spot contribution and 0.6% of sediment input, melted at 9% (Figure 10b). The SE Nicaragua mean is controlled by the enriched composition of the two southernmost volcanoes of Conception and Maderas. This segment requires a DM metasomatized by 0.4% Galapagos hot spot contribution and 0.4% sediment input melted at 6% (Figure 10c). Because of the strong geochemical gradient in SE Nicaragua, the mean value provided here is less appropriate than the means for the other segments. Therefore, the last estimates should be carefully examined in the future. NW Nicaragua requires DM to be metasomatized by 0.6% of sediment melt (and possibly fluids), a melt fraction of 8%, and there is no need for Galapagos hot spot contribution (Figure 10d).

[40] In the Oligocene-Middle Miocene samples the Galapagos hot spot contribution is absent or negligible (Figure 10e). It is not until the Late Miocene-Pliocene that a metasomatic process involving the Galapagos hot spot melts is necessary to explain the trace element data (Figure 10f).

[41] *Carr et al.* [1990] reported a contradictory inverse correlation between degree of melting and volcano size in Central America. The degree of melting was inferred from the REE patterns and was considered high in Nicaragua and low in central Costa Rica. This conclusion was based on the assumption that source composition was the same along the volcanic front. However, a second important observation from the trace element modeling (Figure 10 and Table 4) is that the melt fraction required to reproduce central Costa Rica is similar to the melt fractions needed in the rest of the volcanic front. Steep REE patterns (high La/Yb) imply a lower degree of melting only if C_0 (equations (1) and (2), Appendix A) is the same for all the magmas. The C_0 modeled here is systematically different along the arc and varies from a DM mantle highly metasomatized by Galapagos tracks melts in central Costa Rica to a DM metasomatized by hydrous fluids and/or sediment melts in NW Nicaragua (Table 4). Therefore, the geochemical variations along the volcanic front (e.g., La/Yb, Ba/La, etc.) reflect the extent and type of metasomatic processes caused by the subducting input not just the degree of partial melting. The higher volcanic volumes in Costa Rica [*Carr et al.*, 2007] are possibly related to a more fertile metasomatized mantle (enriched veins from melts of the subducting Galapagos hot spot tracks). While in Nicaragua the Galapagos hot spot contribution is subordinate or insignificant and the resulting metasomatized mantle will be less fertile. Melting of this mantle will produce volcanoes with smaller volumes in Nicaragua.

[42] The main purpose of the modeling presented here was to estimate the effect of the interaction for the Galapagos hot spot with the arc in southern Central America. Our models have several limita-

tions; for example, they do not include the effect of hydrous fluids and fractional crystallization of the primary magmas. According to *Eiler et al.* [2005] a hydrous fluid dominates the slab component in the Nicaraguan volcanic front. Therefore, constraining and modeling the effect of this component will likely refine the fits in some of fluid mobile elements (e.g., Ba, U, K, Pb, and Sr in Figure 10). Missfits occur in P, Zr, and Ti but could be explained by fractional crystallization of apatite (P) and titano-magentite/illmenite (Zr, Ti), possibly at crustal levels. Given the limitations of the modeling, the isotopic and trace element models of the Galapagos hot spot contributions along the volcanic front are remarkably similar and the excellent fits in the central Costa Rica segment argue for an arc–hot spot interaction model.

4.5. Evaluation of the Previous Models That Explain the Galapagos-OIB Signature in Southern Central America

[43] *Russo and Silver* [1994] suggested that a trench-parallel flow of Pacific mantle through the Nazca Plate may feed the growing reservoir of the Atlantic mantle. *Herrstrom et al.* [1995] used this model to explain the enriched nature of the central Costa Rica lavas. However, the maximum $^{208}Pb/^{204}Pb$ signal is not present in eastern Panama (Figure 7), as would be expected for northward flow beneath the Nazca Plate but is instead present in the central Costa Rican volcanic front, directly below the projected subduction of the Galapagos hot spot Seamount Province (Figure 1).

[44] *Abratis and Wörner* [2001] proposed that a slab window in the subducting Cocos-Nazca plates, proposed by *Johnston and Thorkelson* [1997], allowed hot Galapagos mantle to rise into the mantle wedge below southern Costa Rica and Panama, producing the enriched geochemical signature in central Costa Rica. The main weakness in this model is that it does not explain the intermediate values found in some of the Early Middle Miocene samples from the Talamanca Range (Figures 6 and 7). A possible variation on this model could involve flow of hot asthenosphere following a detachment of the subducting slab, as suggested by the OIB magmas in the Trans-Mexican volcanic belt [*Ferrari*, 2004; *Orozco-Esquivel et al.*, 2007]. In this model, the interaction will be between upwelling asthenosphere following the slab detachment and the subducting Seamount Province and the Cocos/Coiba Ridge. Models that suggest direct flow from the Galapagos hot spot plume below southern Costa Rica and Panama via a slab or slab detachment remain interesting ideas whose implications need to be defined and tested.

[45] The oceanic complexes of the Pacific shore of Costa Rica are related to the Caribbean Large Igneous Province (CLIP) and are interpreted to have originated at the Galapagos hot spot [e.g., *Hauff et al.*, 2000; *Hoernle et al.*, 2002; *Denyer et al.*, 2006]. The Costa Rican volcanic front developed on the westernmost part of the CLIP. This geologic history and the high Pb isotopic ratios in eastern Nicaragua and Costa Rican back-arc lavas led *Feigenson et al.* [2004] to propose that the Galapagos-OIB signature is produced by melting CLIP mantle. Our new data contradict this model because we found that the OIB signature is a recent development (Middle Miocene in the Talamanca Range, Late Miocene-Pliocene in central Costa Rica; Figures 5 and 6). If residual CLIP had melted, we would expect the Galapagos-OIB signature to be present since the Oligocene (or even earlier). Also, samples <6 Ma in the central Costa Rica are more enriched in $^{208}Pb/^{204}Pb$ and lower in $^{143}Nd/^{144}Nd$ at a given $^{206}Pb/^{204}Pb$ than the fore-arc CLIP complexes of the Costa Rican Pacific shore (Figure 7). Therefore, melting residual CLIP mantle is not a good source for the OIB signature in southern Central America.

[46] *Goss and Kay* [2006] proposed that the Galapagos-OIB signature results from incorporating portions of the CLIP fore-arc oceanic complexes into the mantle wedge by tectonic erosion. This model can explain the timing of the appearance of the enriched geochemical signature in central Costa Rica lavas only if tectonic erosion initiated with subduction of the Galapagos tracks. However, as mentioned in the preceding paragraph, samples <6 Ma in the central Costa Rica are more enriched in $^{208}Pb/^{204}Pb$ and lower in $^{143}Nd/^{144}Nd$ at a given $^{206}Pb/^{204}Pb$ than the fore-arc CLIP complexes of the Costa Rican fore-arc CLIP complexes. Furthermore, the modern Costa Rican volcanic front and alkaline basalts require a Seamount Province component (Figure 7). As a result, the *Goss and Kay* [2006] model does not explain the isotope and trace element geochemistry of the Late Miocene-recent volcanic in central Costa Rica.

5. Conclusions

[47] Most of the Oligocene-Middle Miocene samples from Costa Rica are normal calc-alkaline arc lavas, geochemically similar to the Nicaraguan

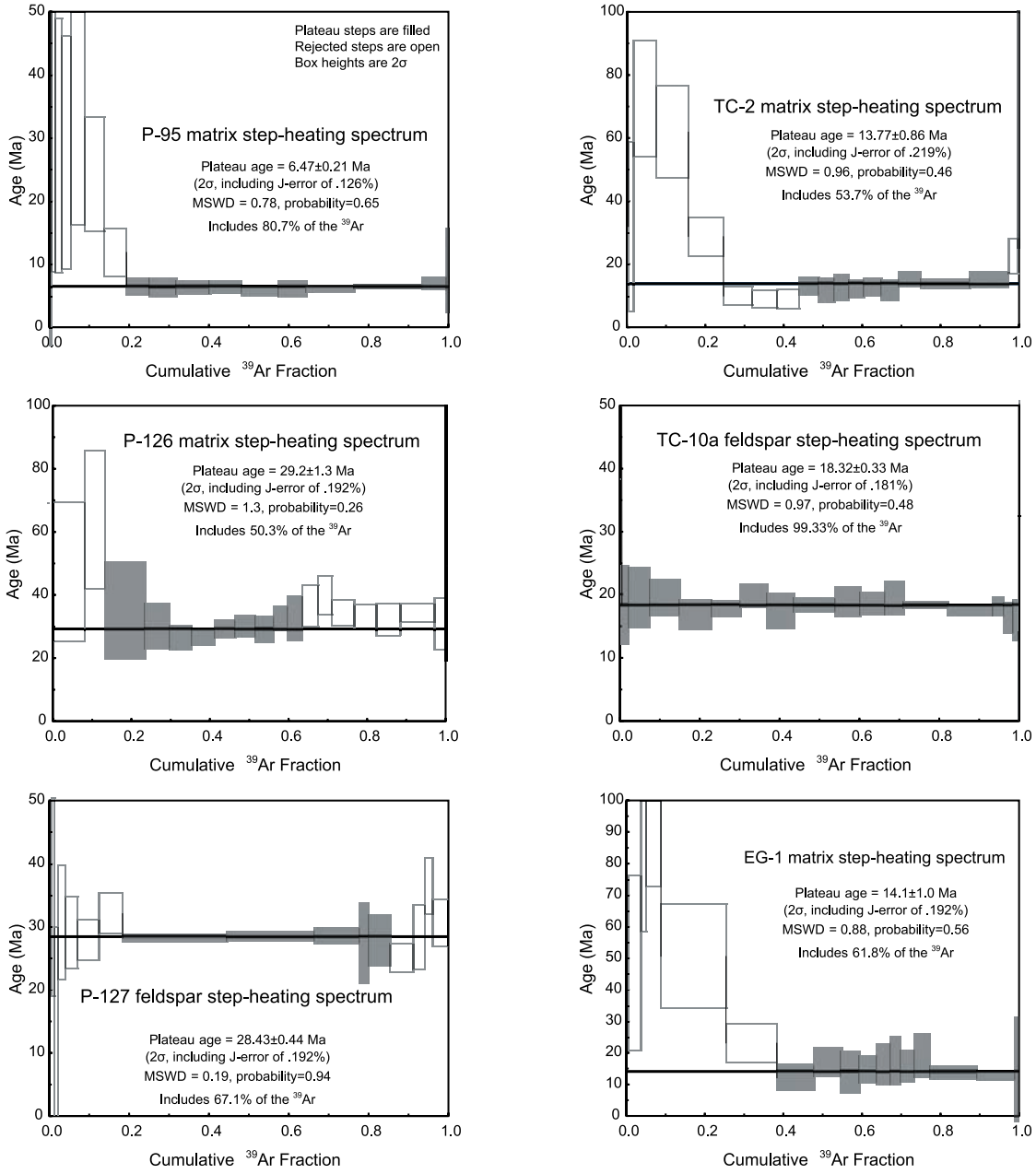

Figure A1. Plateaus spectra for the new $^{40}Ar/^{39}Ar$ dates reported in Table 1.

volcanic front The modern central Costa Rican Galapagos-OIB signature ($^{206}Pb/^{204}Pb > 18.8$, $^{143}Nd/^{144}Nd < 0.513$, LaYb > 10) is evident in the units younger than 6 Ma ago. We propose that this anomalous signature is the result of metasomatic processes related with the subduction of Galapagos hot spot tracks that most likely began to collide with the margin ~8 Ma ago. The intermediate values ($^{206}Pb/^{204}Pb = 18.7–18.8$, La/Yb = 6–10) of some of the samples from the Middle Miocene could represent the effect of the interaction of older Galapagos hot spot tracks that collided with the southern Central American margin during the Miocene.

[48] The southern part of the Central American margin has been interacting with the Galapagos hot spot throughout its geologic history. The relatively recent interaction of the subducting Galapagos hot spot tracks (the Seamount Province, the Cocos/Coiba Ridge, and possible older Galapagos tracks) with the mantle wedge has changed the composition of the erupted lavas in southern Cen-

Table A1. Supplementary Data for the $^{40}Ar/^{39}Ar$ Dates Reported in Table 1[a]

Heating Step	Laser Power [W]	40Ar/ 39Ar	37Ar/ 39Ar	36Ar/ 39Ar	Mol 39ArK	Ca/K	% 40ArA	Cum 39ArK	Age [Ma]	2 Sigma
P-95 Matrix Step-Heating Analysis[b]										
1	0.15	5.70E+03	−1.55E+00	1.92E+01	1.08E-17	−3.0	99.7	5.540E-05	9.84E+01	7.41E+02
2	0.25	4.71E+03	4.11E+00	1.58E+01	1.05E-16	8.1	99.5	5.957E-04	1.68E+02	3.25E+02
3	0.40	1.10E+03	2.86E+00	3.71E+00	8.58E-16	5.6	99.4	5.003E-03	4.78E+01	5.06E+01
4	0.50	2.83E+02	2.67E+00	9.44E-01	1.87E-15	5.2	98.3	1.459E-02	3.21E+01	2.31E+01
5	0.60	1.07E+02	2.84E+00	3.47E-01	2.99E-15	5.6	96.0	2.996E-02	2.89E+01	2.01E+01
6	0.70	1.50E+02	3.59E+00	4.96E-01	4.53E-15	7.1	97.3	5.323E-02	2.78E+01	1.84E+01
7	0.80	1.83E+02	4.03E+00	6.05E-01	6.70E-15	7.9	97.2	8.767E-02	3.44E+01	1.82E+01
8	0.90	1.12E+02	2.79E+00	3.67E-01	9.43E-15	5.5	96.8	1.361E-01	2.43E+01	9.04E+00
9	1.00	4.58E+01	1.92E+00	1.50E-01	1.10E-14	3.8	96.1	1.927E-01	1.20E+01	3.78E+00
10	**1.10**	**1.78E+01**	**1.46E+00**	**5.76E-02**	**1.13E-14**	**2.9**	**94.5**	**2.508E-01**	**6.57E+00**	**1.31E+00**
11	**1.20**	**9.79E+00**	**1.26E+00**	**3.04E-02**	**1.29E-14**	**2.5**	**90.1**	**3.169E-01**	**6.53E+00**	**1.47E+00**
12	**1.35**	**5.93E+00**	**1.10E+00**	**1.73E-02**	**1.63E-14**	**2.2**	**84.0**	**4.008E-01**	**6.41E+00**	**9.49E-01**
13	**1.50**	**4.33E+00**	**1.01E+00**	**1.18E-02**	**1.55E-14**	**2.0**	**77.9**	**4.802E-01**	**6.48E+00**	**9.25E-01**
14	**2.00**	**4.15E+00**	**1.48E+00**	**1.17E-02**	**1.83E-14**	**2.9**	**78.9**	**5.741E-01**	**5.93E+00**	**7.85E-01**
15	**3.00**	**4.56E+00**	**3.97E+00**	**1.41E-02**	**1.35E-14**	**7.8**	**79.8**	**6.436E-01**	**6.23E+00**	**1.21E+00**
16	**5.00**	**3.80E+00**	**3.50E+00**	**1.13E-02**	**2.31E-14**	**6.9**	**76.0**	**7.624E-01**	**6.19E+00**	**4.51E-01**
17	**10.00**	**3.45E+00**	**3.98E+00**	**1.01E-02**	**3.34E-14**	**7.8**	**71.7**	**9.340E-01**	**6.63E+00**	**3.06E-01**
18	**20.00**	**3.36E+00**	**5.81E+00**	**1.04E-02**	**1.16E-14**	**11.4**	**68.9**	**9.934E-01**	**7.10E+00**	**1.01E+00**
19	**25.00**	**3.54E+00**	**6.20E+00**	**1.01E-02**	**1.22E-15**	**12.2**	**61.9**	**9.997E-01**	**9.16E+00**	**6.60E+00**
20	27.50	−6.81E-01	1.19E+01	−3.90E-02	5.89E-17	23.6	1908.4	1.000E+00	8.29E+01	1.62E+02
P-126 Matrix Step-Heating Analysis[c]										
1	0.15	2.91E+01	9.33E-01	7.49E-02	3.53E-15	1.8	75.6	8.079E-02	4.75E+01	2.20E+01
2	0.25	4.77E+01	1.77E+00	1.30E-01	2.23E-15	3.5	79.8	1.318E-01	6.40E+01	2.18E+01
3	**0.40**	**1.95E+01**	**2.08E+00**	**4.91E-02**	**4.40E-15**	**4.1**	**73.0**	**2.326E-01**	**3.52E+01**	**1.53E+01**
4	**0.50**	**1.34E+01**	**3.56E+00**	**3.15E-02**	**2.77E-15**	**7.0**	**66.2**	**2.960E-01**	**3.03E+01**	**7.08E+00**
5	**0.60**	**1.07E+01**	**5.39E+00**	**2.53E-02**	**2.53E-15**	**10.6**	**63.1**	**3.539E-01**	**2.67E+01**	**3.88E+00**
6	**0.70**	**1.03E+01**	**6.76E+00**	**2.43E-02**	**2.49E-15**	**13.3**	**61.0**	**4.109E-01**	**2.71E+01**	**2.65E+00**
7	**0.80**	**1.21E+01**	**7.73E+00**	**2.96E-02**	**2.31E-15**	**15.3**	**64.0**	**4.637E-01**	**2.94E+01**	**2.78E+00**
8	**0.90**	**1.60E+01**	**8.09E+00**	**4.24E-02**	**2.21E-15**	**16.0**	**71.9**	**5.143E-01**	**3.03E+01**	**3.46E+00**
9	**1.00**	**2.18E+01**	**9.19E+00**	**6.30E-02**	**2.02E-15**	**18.2**	**80.1**	**5.604E-01**	**2.93E+01**	**3.97E+00**
10	**1.10**	**2.57E+01**	**9.37E+00**	**7.47E-02**	**1.63E-15**	**18.5**	**81.1**	**5.977E-01**	**3.29E+01**	**3.83E+00**
11	**1.20**	**2.87E+01**	**9.79E+00**	**8.51E-02**	**1.60E-15**	**19.4**	**83.0**	**6.343E-01**	**3.29E+01**	**7.05E+00**
12	1.35	3.17E+01	1.11E+01	9.36E-02	1.75E-15	22.0	82.8	6.743E-01	3.68E+01	6.56E+00
13	1.50	3.38E+01	1.11E+01	9.90E-02	1.49E-15	21.9	82.3	7.085E-01	4.02E+01	6.13E+00
14	2.00	3.54E+01	1.37E+01	1.09E-01	2.57E-15	27.2	85.6	7.673E-01	3.45E+01	3.93E+00
15	3.00	3.61E+01	1.29E+01	1.11E-01	2.44E-15	25.6	86.4	8.231E-01	3.32E+01	3.95E+00
16	5.00	3.33E+01	1.26E+01	1.02E-01	2.66E-15	25.0	85.7	8.841E-01	3.24E+01	5.05E+00
17	10.00	3.25E+01	1.34E+01	9.86E-02	3.79E-15	26.6	84.3	9.708E-01	3.45E+01	2.89E+00
18	20.00	3.30E+01	1.38E+01	1.02E-01	1.22E-15	27.5	86.2	9.987E-01	3.09E+01	8.13E+00
19	25.00	3.58E+01	2.16E+01	7.34E-02	5.50E-17	43.2	52.6	1.000E+00	1.13E+02	9.40E+01
20	>	−1.68E+02	−4.35E+01	−1.02E-01	−5.46E-18	−81.8	14.6	1.000E+00	−1.30E+03	3.94E+03
P-127 Feldspar Step-Heating Analysis[d]										
1	0.15	6.61E+02	2.05E+00	1.93E+00	2.97E-18	4.0	86.1	6.293E-05	5.34E+02	1.41E+03
2	0.25	5.49E+03	7.32E+01	1.80E+01	3.09E-18	154.7	96.9	1.284E-04	9.52E+02	1.75E+03
3	0.40	3.39E+03	1.91E+01	1.13E+01	3.25E-17	38.2	98.6	8.161E-04	2.95E+02	3.84E+02
4	0.50	3.01E+03	1.28E+01	9.88E+00	2.74E-17	25.5	96.8	1.397E-03	5.65E+02	1.69E+02
5	0.60	1.51E+03	8.98E+00	5.02E+00	4.02E-17	17.8	98.0	2.248E-03	2.00E+02	3.11E+02
6	0.80	5.67E+02	7.71E+00	1.92E+00	1.51E-16	15.2	99.9	5.449E-03	2.67E+00	9.42E+01
7	1.00	1.27E+02	7.42E+00	4.12E-01	3.13E-16	14.7	95.5	1.208E-02	3.84E+01	1.93E+01
8	1.20	3.83E+01	7.45E+00	1.28E-01	4.44E-16	14.7	95.9	2.149E-02	1.06E+01	1.95E+01
9	1.50	1.74E+01	7.13E+00	4.65E-02	8.54E-16	14.1	73.7	3.957E-02	3.08E+01	9.01E+00
10	2.00	6.04E+00	6.97E+00	8.84E-03	1.44E-15	13.8	28.2	7.000E-02	2.92E+01	5.64E+00
11	3.00	5.00E+00	6.92E+00	5.92E-03	2.55E-15	13.7	16.9	1.240E-01	2.80E+01	3.19E+00
12	4.00	4.67E+00	8.14E+00	3.24E-03	2.77E-15	16.1	−2.3	1.826E-01	3.22E+01	3.23E+00
13	**6.00**	**4.32E+00**	**8.80E+00**	**4.32E-03**	**1.24E-14**	**17.4**	**2.9**	**4.446E-01**	**2.83E+01**	**6.12E-01**
14	**8.00**	**4.22E+00**	**9.30E+00**	**4.06E-03**	**1.03E-14**	**18.4**	**−0.4**	**6.632E-01**	**2.86E+01**	**7.36E-01**

Table A1. (continued)

Heating Step	Laser Power [W]	40Ar/ 39Ar	37Ar/ 39Ar	36Ar/ 39Ar	Mol 39ArK	Ca/K	% 40ArA	Cum 39ArK	Age [Ma]	2 Sigma
15	**10.00**	**4.19E+00**	**8.80E+00**	**3.73E-03**	**5.38E-15**	**17.4**	**−1.1**	**7.771E-01**	**2.86E+01**	**1.21E+00**
16	**12.00**	**4.20E+00**	**8.81E+00**	**4.34E-03**	**1.06E-15**	**17.4**	**3.2**	**7.994E-01**	**2.74E+01**	**6.35E+00**
17	**15.00**	**4.19E+00**	**8.92E+00**	**4.16E-03**	**2.55E-15**	**17.6**	**1.5**	**8.535E-01**	**2.79E+01**	**3.97E+00**
18	20.00	4.20E+00	9.27E+00	5.75E-03	2.71E-15	18.3	11.6	9.110E-01	2.51E+01	2.30E+00
19	25.00	4.20E+00	9.13E+00	4.00E-03	1.43E-15	18.1	−0.2	9.412E-01	2.84E+01	5.09E+00
20	>	4.20E+00	9.04E+00	−1.43E-04	9.07E-16	17.9	−29.2	9.604E-01	3.65E+01	4.48E+00
21	≫	4.22E+00	9.21E+00	2.97E-03	1.81E-15	18.2	−7.7	9.988E-01	3.06E+01	3.66E+00
22	⋙	4.15E+00	7.63E+00	2.37E-02	5.74E-17	15.1	145.2	1.000E+00	−1.28E+01	9.98E+01
				EG-1 Matrix Step-Heating Analysis[e]						
1	0.15	6.96E+03	4.40E+00	2.34E+01	4.46E-17	8.7	99.2	1.073E-03	3.57E+02	2.38E+02
2	0.25	2.32E+03	5.70E+00	7.81E+00	1.66E-16	11.2	99.4	5.055E-03	8.85E+01	1.17E+02
3	0.40	6.13E+02	5.20E+00	2.05E+00	1.28E-15	10.2	98.8	3.573E-02	4.87E+01	2.76E+01
4	0.50	2.73E+02	3.34E+00	8.76E-01	5.58E-16	6.6	94.5	4.914E-02	9.82E+01	3.95E+01
5	0.60	1.71E+02	2.92E+00	5.24E-01	1.56E-15	5.7	90.6	8.660E-02	1.05E+02	3.22E+01
6	0.70	1.88E+02	3.72E+00	6.11E-01	6.90E-15	7.3	95.9	2.526E-01	5.08E+01	1.64E+01
7	0.80	6.33E+01	4.33E+00	2.04E-01	5.38E-15	8.5	94.5	3.821E-01	2.34E+01	6.17E+00
8	**0.90**	**2.91E+01**	**3.93E+00**	**9.40E-02**	**3.91E-15**	**7.7**	**93.7**	**4.761E-01**	**1.24E+01**	**4.06E+00**
9	**1.00**	**1.99E+01**	**3.75E+00**	**6.01E-02**	**2.90E-15**	**7.4**	**87.0**	**5.458E-01**	**1.74E+01**	**4.54E+00**
10	**1.10**	**1.64E+01**	**3.45E+00**	**4.98E-02**	**1.95E-15**	**6.8**	**87.2**	**5.928E-01**	**1.41E+01**	**6.47E+00**
11	**1.20**	**1.48E+01**	**3.63E+00**	**4.43E-02**	**1.77E-15**	**7.1**	**85.1**	**6.355E-01**	**1.49E+01**	**4.26E+00**
12	**1.35**	**1.47E+01**	**4.70E+00**	**4.35E-02**	**1.49E-15**	**9.3**	**83.2**	**6.714E-01**	**1.67E+01**	**6.47E+00**
13	**1.50**	**1.45E+01**	**6.04E+00**	**4.29E-02**	**1.07E-15**	**11.9**	**81.9**	**6.971E-01**	**1.77E+01**	**7.58E+00**
14	**2.00**	**1.52E+01**	**1.00E+01**	**4.78E-02**	**1.55E-15**	**19.8**	**84.5**	**7.344E-01**	**1.60E+01**	**4.95E+00**
15	**3.00**	**1.37E+01**	**1.42E+01**	**4.31E-02**	**1.62E-15**	**28.2**	**79.3**	**7.734E-01**	**1.94E+01**	**6.84E+00**
16	**5.00**	**1.02E+01**	**1.48E+01**	**3.39E-02**	**4.90E-15**	**29.4**	**79.6**	**8.914E-01**	**1.41E+01**	**2.02E+00**
17	**10.00**	**9.51E+00**	**2.44E+01**	**3.65E-02**	**4.05E-15**	**48.9**	**80.0**	**9.888E-01**	**1.31E+01**	**1.53E+00**
18	**20.00**	**1.08E+01**	**4.09E+01**	**4.75E-02**	**4.34E-16**	**83.5**	**80.3**	**9.992E-01**	**1.50E+01**	**1.64E+01**
19	**25.00**	**1.71E+01**	**6.97E+01**	**6.45E-02**	**3.38E-17**	**146.8**	**58.2**	**1.000E+00**	**5.11E+01**	**1.05E+02**
20	>	1.02E+01	7.65E-01	9.93E-03	−1.92E-17	1.5	27.8	1.000E+00	4.90E+01	2.95E+02
				TC-2 Matrix Step-Heating Analysis[f]						
1	0.13	1.69E+03	7.64E+00	5.63E+00	1.16E-16	15.1	98.2	2.469E-03	1.83E+02	7.44E+01
2	0.20	3.90E+02	6.73E+00	1.30E+00	6.70E-16	13.3	98.7	1.678E-02	3.21E+01	2.69E+01
3	0.30	7.94E+01	4.17E+00	2.31E-01	2.73E-15	8.2	85.1	7.503E-02	7.25E+01	1.84E+01
4	0.40	5.37E+01	4.24E+00	1.50E-01	3.79E-15	8.3	81.3	1.559E-01	6.20E+01	1.46E+01
5	0.50	3.17E+01	3.60E+00	9.32E-02	4.21E-15	7.1	85.3	2.458E-01	2.90E+01	6.12E+00
6	0.60	1.20E+01	3.19E+00	3.66E-02	3.40E-15	6.3	86.4	3.183E-01	1.02E+01	3.00E+00
7	0.70	8.81E+00	2.74E+00	2.60E-02	3.03E-15	5.4	83.2	3.830E-01	9.22E+00	2.87E+00
8	0.80	9.03E+00	2.66E+00	2.66E-02	2.59E-15	5.2	83.4	4.383E-01	9.34E+00	3.06E+00
9	**0.90**	**8.74E+00**	**2.91E+00**	**2.36E-02**	**2.31E-15**	**5.7**	**75.5**	**4.877E-01**	**1.33E+01**	**2.77E+00**
10	**1.00**	**9.39E+00**	**3.02E+00**	**2.66E-02**	**1.93E-15**	**5.9**	**79.5**	**5.290E-01**	**1.20E+01**	**3.79E+00**
11	**1.10**	**9.73E+00**	**3.23E+00**	**2.73E-02**	**1.73E-15**	**6.3**	**78.8**	**5.660E-01**	**1.29E+01**	**4.13E+00**
12	**1.20**	**9.23E+00**	**3.03E+00**	**2.59E-02**	**1.83E-15**	**5.9**	**78.6**	**6.051E-01**	**1.23E+01**	**2.73E+00**
13	**1.35**	**9.40E+00**	**3.17E+00**	**2.61E-02**	**2.04E-15**	**6.2**	**77.9**	**6.486E-01**	**1.30E+01**	**2.80E+00**
14	**1.50**	**9.24E+00**	**3.68E+00**	**2.64E-02**	**2.08E-15**	**7.2**	**79.2**	**6.930E-01**	**1.20E+01**	**3.26E+00**
15	**2.00**	**8.46E+00**	**3.33E+00**	**2.17E-02**	**2.65E-15**	**6.5**	**70.7**	**7.497E-01**	**1.54E+01**	**2.36E+00**
16	**3.00**	**1.18E+01**	**3.78E+00**	**3.38E-02**	**5.86E-15**	**7.4**	**80.8**	**8.748E-01**	**1.41E+01**	**1.58E+00**
17	**5.00**	**1.66E+01**	**4.78E+00**	**5.00E-02**	**4.70E-15**	**9.4**	**85.1**	**9.752E-01**	**1.55E+01**	**2.48E+00**
18	10.00	2.15E+01	7.24E+00	6.37E-02	1.07E-15	14.3	83.0	9.981E-01	2.28E+01	5.64E+00
19	15.00	2.13E+01	6.51E+00	3.31E-02	8.88E-17	12.8	41.9	1.000E+00	7.62E+01	5.07E+01
20	20.00	−9.19E+01	−2.96E+01	−4.00E-01	−6.01E-18	−56.5	124.5	1.000E+00	1.32E+02	5.50E+02
				TC-10a Feldspar Step-Heating Analysis[g]						
1	0.13	5.49E+02	2.07E+00	1.82E+00	5.22E-16	4.1	98.0	3.704E-03	6.97E+01	3.13E+01
2	**0.20**	**1.11E+02**	**9.78E-01**	**3.67E-01**	**2.35E-15**	**1.9**	**97.5**	**2.037E-02**	**1.85E+01**	**6.18E+00**
3	**0.30**	**5.09E+01**	**8.56E-01**	**1.62E-01**	**7.53E-15**	**1.7**	**94.1**	**7.378E-02**	**1.96E+01**	**4.73E+00**
4	**0.40**	**3.85E+01**	**1.12E+00**	**1.21E-01**	**1.05E-14**	**2.2**	**92.2**	**1.484E-01**	**1.96E+01**	**2.82E+00**

Table A1. (continued)

Heating Step	Laser Power [W]	40Ar/ 39Ar	37Ar/ 39Ar	36Ar/ 39Ar	Mol 39ArK	Ca/K	% 40ArA	Cum 39ArK	Age [Ma]	2 Sigma
5	**0.50**	**2.93E+01**	**1.21E+00**	**9.08E-02**	**1.12E-14**	**2.4**	**91.1**	**2.279E-01**	**1.70E+01**	**2.35E+00**
6	**0.60**	**3.14E+01**	**1.01E+00**	**9.73E-02**	**1.02E-14**	**2.0**	**91.3**	**3.004E-01**	**1.78E+01**	**1.27E+00**
7	**0.70**	**3.13E+01**	**1.13E+00**	**9.62E-02**	**9.46E-15**	**2.2**	**90.3**	**3.674E-01**	**1.99E+01**	**1.82E+00**
8	**0.80**	**2.49E+01**	**1.55E+00**	**7.58E-02**	**9.49E-15**	**3.0**	**89.2**	**4.347E-01**	**1.75E+01**	**2.75E+00**
9	**1.00**	**2.36E+01**	**1.49E+00**	**7.09E-02**	**1.45E-14**	**2.9**	**88.0**	**5.376E-01**	**1.85E+01**	**1.04E+00**
10	**1.20**	**2.37E+01**	**1.25E+00**	**7.08E-02**	**8.95E-15**	**2.5**	**87.7**	**6.011E-01**	**1.90E+01**	**2.31E+00**
11	**1.35**	**2.44E+01**	**1.26E+00**	**7.34E-02**	**8.76E-15**	**2.5**	**88.2**	**6.632E-01**	**1.87E+01**	**1.77E+00**
12	**1.50**	**2.63E+01**	**9.25E-01**	**7.91E-02**	**6.58E-15**	**1.8**	**88.5**	**7.099E-01**	**1.96E+01**	**2.61E+00**
13	**2.00**	**1.63E+01**	**8.90E-01**	**4.59E-02**	**1.55E-14**	**1.7**	**82.6**	**8.200E-01**	**1.85E+01**	**4.83E-01**
14	**3.00**	**1.45E+01**	**1.18E+00**	**4.05E-02**	**1.59E-14**	**2.3**	**81.3**	**9.330E-01**	**1.77E+01**	**9.19E-01**
15	**4.00**	**1.13E+01**	**1.46E+00**	**2.95E-02**	**3.81E-15**	**2.9**	**75.2**	**9.600E-01**	**1.83E+01**	**1.48E+00**
16	**6.00**	**1.13E+01**	**8.61E-01**	**3.01E-02**	**3.43E-15**	**1.7**	**77.7**	**9.843E-01**	**1.64E+01**	**2.40E+00**
17	**8.00**	**1.10E+01**	**6.73E-01**	**2.90E-02**	**1.79E-15**	**1.3**	**77.5**	**9.970E-01**	**1.61E+01**	**3.23E+00**
18	10.00	1.27E+01	1.79E+00	4.40E-02	2.98E-16	3.5	100.9	9.991E-01	−7.44E-01	1.50E+01
19	12.00	1.48E+01	1.33E+00	7.73E-02	4.99E-17	2.6	153.4	9.995E-01	−5.24E+01	8.50E+01
20	15.00	1.05E+01	2.37E+00	4.12E-02	7.32E-17	4.6	112.9	1.000E+00	−8.88E+00	5.96E+01

[a] The plateau steps are shown in bold.

[b] For P-95 matrix step-heating analysis, mass is 8.513 mg, J = 3.75E-03 ± 4.72E-06 ± 0.126 Percent; 2 Sigma). Total gas age is 9.98 ± 0.21 Ma (2s, steps 1 through 20). Total isochron age is 6.23 ± 0.29 Ma (2s, steps 1 through 20) and initial 40Ar/36Ar is 298.89 ± 0.73 where MSWD = 1.529. Plateau age is 6.47 ± 0.21 Ma (2s, including J-error of 0.126%), stats are MSWD = 0.78, probability = 0.65, and size is 80.7% of the 39Ar, steps 10 through 20.

[c] For P-126 matrix step-heating analysis, mass is 6.528 mg, J = 3.74E-03 ± 7.19E-06 (0.192 Percent; 2 Sigma). Total gas age is 35.2 ± 1.0 Ma (2s, steps 1 through 20). Isochron age is 25.80 ± 0.27 Ma (2s, steps 1 through 20) and initial 40Ar/36Ar is 309.50 ± 6.00, where MSWD = 1.50. Plateau age is 29.2 ± 1.3 Ma (2s, including J-error of 0.192%), stats are MSWD = 1.3, probability = 0.26, and size is 50.3% of the 39Ar, steps 3 through 11.

[d] For P-127 feldspar step-heating analysis, mass is 6.441 mg and J = 3.74E-03 ± 7.19E-06 (0.192 Percent; 2 Sigma). Total gas age is 29.2 ± 0.4 Ma (2s, steps 1 through 22). Isochron age is 28.44 ± 0.64 Ma (2s, steps 1 through 22), and initial 40Ar/36Ar is 302.50 ± 3.16, where MSWD = 2.30. Plateau age is 28.43 ± 0.44 Ma (2s, including J-error of 0.192%), stats are MSWD = 0.19, probability = 0.94, and size is 67.1% of the 39Ar, steps 13 through 17.

[e] For EG-1 matrix step-heating analysis, mass is 6.023 mg and J = 3.74E-03 ± 7.19E-06 (0.192 Percent; 2 Sigma). Total gas age is 28.1 ± 1.0 Ma (2s, steps 1 through 20). Isochron age is 13.57 ± 2.24 Ma (2s, steps 1 through 20) and initial 40Ar/36Ar is 299.30 ± 2.26, where MSWD = 4.35. Plateau age is 14.1 ± 1 Ma (2s, including J-error of 0.192%), stats are MSWD = 0.88, probability = 0.56, and size is 61.8% of the 39Ar, steps 8 through 19.

[f] For TC-2 matrix step-heating analysis, mass is 1.540 mg and J = 3.46E-03 ± 7.57E-06 (0.219 Percent; 2 Sigma). Total gas age is 22.7 ± 0.8 Ma (2s, steps 1 through 20). Isochron age is 12.33 ± 2.48 Ma (2s, steps 1 through 20), and initial 40Ar/36Ar is 302.50 ± 5.47 MSWD = 8.18. Plateau age is 13.77 ± 0.86 Ma (2s, including J-error of 0.219%), stats are MSWD = 0.96, probability = 0.46, and size is 53.7% of the 39Ar, steps 9 through 17.

[g] For TC-10a feldspar step-heating analysis, mass is 1.349 mg and J = 3.63E-03 ± 6.55E-06 (0.181 Percent; 2 Sigma). Total gas age is 18.5 ± 0.3 Ma (2s, steps 1 through 20). Isochron age is 17.55 ± 0.80 Ma (2s, steps 1 through 20) and initial 40Ar/36Ar is 297.60 ± 1.88, where MSWD = 1.47. Plateau age is 18.32 ± 0.33 Ma (2s, including J-error of 0.181%), stats are MSWD = 0.97, probability = 0.48, and size is 99.3% of the 39Ar, steps 2 through 17.

tral America producing a hot spot signature (Galapagos-OIB) in a volcanic arc.

[49] The Galapagos hot spot contribution is mix between the volumetrically major Cocos/Coiba Ridge component and the highly enriched Seamount Province. The most enriched isotopic signature is present in central Costa Rica, directly above the subducting Seamount Province. There is a systematic decrease in the influence of the Galapagos hot spot along the volcanic front from central Costa Rica to NW Nicaragua. The interaction of the southern Central American segments of the arc with the eruptive products of the Galapagos hot spot, subducting beneath Costa Rica, is strongly favored by the geochemical and geochronological data presented here, therefore more complex models are not required.

Appendix A

[50] Appendix A contains 2Figure A1 and Tables A1 and A2.

Acknowledgments

[51] Field work logistics supported by P. Denyer, G. Alvarado, and T. Aguilar from the Central American School of Geology at the University of Costa Rica. Revisions by L. Patino, I. Saginor, N. Sou, and S. Whattam improved the manuscript. Reviews and comments by I. Smith, O. Ishizuka, and V. Salters are highly appreciated. This research is the

Table A2 (Sample). Modeled Components and Melts for the Southern Central American Lavas[a] [The full Table A2 is available in the HTML version of this article at http://www.g-cubed.org]

Model	Rb	Ba	Th	U	Nb	Ta	K_2O	La	Ce	Pb	Pr	Sr	P_2O_5	Nd	Zr	Sm	Eu
DM (SO 144-1) 8%F (60ol25opx12cpx3spn)	0.061	0.491	0.007	0.002	0.114	0.008	0.006	0.190	0.645	0.046	0.125	8.499	0.009	0.718	6.733	0.300	0.114
Mean Semount Province melt (SP) 20%F (83cpx15ga2rut)	174.700	2094.676	21.047	8.438	62.217	3.268	8.600	190.473	353.951	10.141	45.302	2755.231	3.148	108.962	265.090	8.209	1.951
Mean Cocos/Coiba Ridge melt (CCR) 20%F (83cpx15ga2ru)	51.400	435.095	6.199	4.444	17.168	0.883	1.650	63.342	120.672	3.396	17.539	974.121	1.849	46.803	122.595	4.445	1.146
Galapagos Component 1 (SP40 + CCR 60%)	100.720	1098.927	12.138	6.042	35.188	1.837	4.430	114.194	213.984	6.094	28.644	1686.565	2.368	71.666	179.593	5.950	1.468
Galapagos Component 2 (SP20% + CCR80%)	76.060	767.011	9.169	5.243	26.178	1.360	3.040	88.768	167.328	4.745	23.092	1330.343	2.108	59.234	151.094	5.197	1.307
Sediment Melt1 (30Carb + 70Hemi) 20%F (D15garnet84.6cpx0.4rut)	149.150	17013.203	10.738	17.313	12.073	0.771	6.710	75.445	91.411	36.251	14.314	3329.281	0.615	38.920	74.387	3.031	1.087
SedMelt 2(Oligocene-Miocene) (30Carb + 70Hemi) 20%F (D15garnet84.6cpx0.4rut)	149.150	5671.060	10.738	3.850	12.073	0.771	6.710	75.445	91.411	12.860	14.314	3329.281	0.615	38.920	74.387	3.031	1.087
Central Costa Rica C_0 (60ol25opx13.5cpx1.5ga)	3.230	50.457	0.382	0.201	1.178	0.064	0.145	3.685	7.136	0.264	0.995	62.162	0.081	2.885	11.986	0.472	0.156
Central Costa Rica C_L	40.371	630.712	4.773	2.511	14.721	0.795	1.813	46.062	89.087	3.299	12.260	769.112	0.971	34.147	134.825	4.870	1.475
NW Costa Rica C_0 (60ol25opx14.5cpx0.5ga)	1.559	109.158	0.144	0.142	0.396	0.024	0.072	1.325	2.470	0.300	0.381	38.492	0.027	1.373	8.176	0.350	0.128
NW Costa Rica C_L	17.325	1212.868	1.604	1.583	4.398	0.262	0.804	14.724	27.420	3.332	4.193	424.387	0.292	14.618	85.780	3.331	1.146
SE Nicaragua C_0 (60ol25opx14.7cpx0.3ga)	1.060	72.936	0.099	0.096	0.302	0.018	0.050	0.947	1.862	0.215	0.296	28.494	0.021	1.155	7.695	0.333	0.124
SE Nicaragua C_L	17.663	1215.597	1.644	1.597	5.024	0.306	0.835	15.770	30.715	3.574	4.681	454.579	0.319	16.801	109.711	3.992	1.354
NW Nicaragua C_0 (60ol25opx14.7cpx0.3ga)	0.955	102.568	0.072	0.106	0.185	0.013	0.046	0.641	1.190	0.264	0.210	28.424	0.013	0.947	7.139	0.316	0.120
NW Nicaragua model C_L	13.247	911.697	1.233	1.197	3.771	0.230	0.626	11.833	23.223	2.691	3.632	351.082	0.253	13.540	89.099	3.413	1.181
Late Miocene-Pliocene $C_0$1(60ol25opx14cpx1ga)	1.335	38.347	0.117	0.052	0.316	0.019	0.061	1.084	2.023	0.147	0.325	35.033	0.023	1.240	7.861	0.341	0.126
Late Miocene-Pliocene C_L1	33.383	958.680	2.935	1.292	7.805	0.478	1.525	26.959	48.439	3.581	7.064	776.119	0.467	23.387	136.179	4.862	1.582
Late Miocene-Pliocene $C_0$2(60ol25opx14cpx1ga)	0.955	34.515	0.072	0.025	0.185	0.013	0.046	0.641	1.190	0.123	0.210	28.424	0.013	0.947	7.139	0.316	0.120
Late Miocene-Pliocene C_L2	23.883	862.865	1.790	0.637	4.583	0.311	1.146	15.945	28.485	3.008	4.568	629.698	0.256	17.869	123.674	4.512	1.507
Oligocene-Pliocene C_0 (60ol25opx14.7cpx0.3ga)	0.955	34.515	0.072	0.025	0.185	0.013	0.046	0.641	1.190	0.123	0.210	28.424	0.013	0.947	7.139	0.316	0.120
Oligocene-Pliocene C_L	11.942	431.433	0.895	0.319	2.317	0.157	0.573	8.014	14.842	1.540	2.580	350.211	0.153	11.108	82.659	3.237	1.147

[a] The melting model used in this study was aggregated fractional melting [*Shaw*, 1970] described by the following equation: $C_L/C_0 = 1/F \times [1 - (1 - F)^{1/D0}]$. Where C_L is the average concentration of the element in the liquid, C_0 is the initial concentration of the element in the source, F is the melt fraction, and D_0 is the initial bulk partition coefficient. Equation (1) is derived from the mass balance equation $C_0 = F \times C_L + (1 - F)C_S$, and the bulk partition coefficient $D = C_S/C_L$. Where C_S is the concentration of the element in the solid phase. The partition coefficients used in our modeling (peridotite and eclogite sources) are from the compilation of *Kelemen et al.* [2003]. The DM composition was inverted from sample SO-144-1 from *Werner et al.* [2003]. Modeled melts in eclogite facies from the subducting Seamount Province and Cocos/Coiba Ridge were based on the average calculation of the data published by *Hoernle et al.* [2000] and *Werner et al.* [2003]. The subducting sediments were obtained from *Patino et al.* [2000] and the melt modeled was produced from a 30% carbonate (carb.) and a 70% hemipelagic (hemi.) sediment mix. Average TiO_2 concentrations in the subducting plate were used as a proxy for rutile in the residue. The trace element patterns are plotted in Figures 8 and 10, and other details of the modeling are in section 4.4. cpx: clinopyroxene, ga:garnet, ol:olivine, opx:orthopyroxene, rut: rutile, spn: spinel. C_0: Composition of the metasomatized mantle, C_L: Composition of the melts from the metazomatized mantle, F: melt fraction in percent.

result of collaboration between the Department of Earth and Planetary Sciences at Rutgers University, IFM-GEOMAR, and Michigan State University. This work was supported through the NSF Margins Program, grants EAR0203388 and NSF OCE 0505924, the German Science Foundation Collaborative Research Center (SFB574, contribution 145), and by the Rutgers University Graduate School Pre-Dissertation award.

References

Abratis, M., and G. Wörner (2001), Ridge collision, slab-window formation, and the flux of Pacific asthenosphere into the Caribbean realm, *Geology*, *29*(2), 127–130, doi:10.1130/0091-7613(2001)029<0127:RCSWFA>2.0.CO;2.

Alvarado, G. E., C. Dengo, U. Martens, J. Bundschuh, T. Aguilar, and S. B. Bonis (2007), Stratigraphy and geologic history, in *Central America: Geology, Resources, and Hazards*, edited by J. Bundschuh and G. E. Alvarado, pp. 345–394, Taylor and Francis, London.

Benjamin, E. R., T. Plank, J. A. Wade, K. A. Kelley, E. H. Hauri, and G. E. Alvarado (2007), High water contents in basaltic magmas from Irazú volcano, Costa Rico, *J. Volcanol. Geotherm. Res.*, *168*, 68–92.

Bindeman, I. N., J. M. Eiler, G. M. Yogodzinski, Y. Tatsumi, C. R. Stern, T. L. Grove, M. Portnyagin, K. Hoernle, and L. V. Danyushevsky (2005), Oxygen isotope evidence for slab melting in modern and ancient subduction zones, *Earth Planet. Sci. Lett.*, *235*, 480–496, doi:10.1016/j.epsl.2005.04.014.

Bryant, J. A., G. M. Yogodzinski, M. L. Hall, J. L. Lewicki, and D. G. Bailey (2006), Geochemical constrains on the origin of volcanic rocks from the Andean northern volcanic zone, Ecuador, *J. Petrol.*, *47*(6), 1147–1175, doi:10.1093/petrology/egl006.

Calvo, C., and A. Bolz (1994), The oldest calc-alkaline island arc volcanism in Costa Rica. Marine tephra from the Loma Chumico Formation (Albian to Campanian), *Profil*, *7*, 235–264.

Carr, M. J., M. D. Feigenson, and E. A. Bennett (1990), Incompatible element and isotopic evidence for tectonic control of source mixing and melt extraction along the Central American arc, *Contrib. Mineral. Petrol.*, *105*, 369–380, doi:10.1007/BF00286825.

Carr, M. J., M. D. Feigenson, L. C. Patino, and J. A. Walker (2003), Volcanism and geochemistry in Central America: Progress and problems, in *Inside the Subduction Factory*, *Geophys. Monogr. Ser.*, vol. 138, edited by J. Eiler and G. Abers, pp. 153–179, AGU, Washington, D. C.

Carr, M. J., I. Saginor, G. E. Alvarado, L. Bolge, F. Lindsay, K. Milidakis, B. Turrin, M. D. Feigenson, and C. C. Swisher, III (2007), Element fluxes from the volcanic front of Nicaragua and Costa Rica, *Geochem. Geophys. Geosyst.*, *8*(6), Q06001, doi:10.1029/2006GC001396.

DeMets, C. (2001), A new estimate for present-day Cocos–Caribbean Plate motion: Implications for slip along the Central American volcanic arc, *Geophys. Res. Lett.*, *28*, 4043–4046, doi:10.1029/2001GL013518.

Denyer, P., and G. E. Alvarado (2007), *Mapa Geologico de Costa Rica*, Liberia Francesa S. S., San Jose, Costa Rica.

Denyer, P., and O. Arias (1991), Estratigrafía de la región central de Costa Rica, *Rev. Geol. Am. Cent.*, *12*, 1–59. (Available at http://www.geologia.ucr.ac.cr/revista-geol.htm)

Denyer, P., P. O. Baumgartner, and E. Gazel (2006), Characterization and tectonic implications of Mesozoic-Cenozoic oceanic assemblages of Costa Rica and Western Panama, *Geol. Acta*, *4*(1–2), 203–218.

Ehrenborg, J. (1996), A new stratigraphy for the Tertiary volcanic rocks of the Nicaraguan Highland, *Geol. Soc. Am. Bull.*, *108*(7), 830–842, doi:10.1130/0016-7606(1996)108<0830:ANSFTT>2.3.CO;2.

Eiler, J. M., M. J. Carr, M. Reagan, and E. Stolper (2005), Oxygen isotope constraints on the sources of Central American arc lavas, *Geochem. Geophys. Geosyst.*, *6*, Q07007, doi:10.1029/2004GC000804.

Faure, G. (1986), *Principles of Isotope Geology*, 2nd ed., 589 pp., John Wiley, New York.

Feigenson, M. D., and M. J. Carr (1986), Positively correlated Nd and Sr isotope ratios of lavas from the Central American volcanic front, *Geology*, *14*, 79–82, doi:10.1130/0091-7613(1986)14<79:PCNASI>2.0.CO;2.

Feigenson, M. D., and M. J. Carr (1993), The source of Central American lavas: Inferences from geochemical inverse modeling, *Contrib. Mineral. Petrol.*, *113*, 226–235, doi:10.1007/BF00283230.

Feigenson, M. D., M. J. Carr, S. V. Maharaj, S. Juliano, and L. L. Bolge (2004), Lead isotope composition of Central American volcanoes: Influence of the Galapagos plume, *Geochem. Geophys. Geosyst.*, *5*, Q06001, doi:10.1029/2003GC000621.

Ferrari, L. (2004), Slab detachment control on mafic volcanic pulses and mantle heterogeneity in Central Mexico, *Geology*, *32*, 77–80, doi:10.1130/G19887.1.

Galer, S. J. G., and W. Abouchami (1998), Practical application of lead triple spiking for correction of instrumental mass discrimination, *Min. Mag.*, *62A*, 491–492, doi:10.1180/minmag.1998.62A.1.260.

Gardner, T. W., D. Verdonk, N. M. Pinter, R. L. Slingerland, K. P. Furlong, T. F. Bullard, and S. G. Wells (1992), Quaternary uplift astride of aseismic Cocos Ridge, Pacific Coast, Costa Rica, *Geol. Soc. Am. Bull.*, *104*, 219–232, doi:10.1130/0016-7606(1992)104<0219:QUATAC>2.3.CO;2.

Gazel, E. (2003), Las series alcalinas del Plioceno de Costa Rica: Distribución espacial y relación con una fuente mantelica tipo OIB, *Rev. Geol. Am. Cent.*, *29*, 87–94.

Gazel, E., G. E. Alvarado, J. Obando, and A. Alfaro (2005), Evolución magmática del arco de Sarapiquí, Costa Rica, *Rev. Geol. Am. Cent.*, *32*, 13–31.

Geldmacher, J., K. Hoernle, A. Klügel, P. van den Bogaard, F. Wombacher, and B. Berning (2006), Origin and geochemical evolution of the Madeira-Tore Rise (eastern north Atlantic), *J. Geophys. Res.*, *111*, B09206, doi:10.1029/2005JB003931.

Goss, A. R., and S. M. Kay (2006), Steep REE patterns and enriched Pb isotopes in southern Central American arc magmas: Evidence for forearc subduction erosion?, *Geochem. Geophys. Geosyst.*, *7*, Q05016, doi:10.1029/2005GC001163.

Gräfe, K., W. Frisch, I. M. Villa, and M. Meschede (2002), Geodynamic evolution of southern Costa Rica related to low-angle subduction of the Cocos Ridge: Constrains from thermochronology, *Tectonophysics*, *348*, 187–204, doi:10.1016/S0040-1951(02)00113-0.

Hannah, R. S., T. A. Vogel, L. C. Patino, and G. E. Alvarado (2002), The Origin of the chemically variable 0.33 Ma Valle Central Ash-flow tuff, Costa Rica, *Bull. Volcanol.*, *64*, 117–133, doi:10.1007/s00445-001-0188-8.

Harpp, K. S., V. Wanless, R. Otto, K. Hoernle, and R. Werner (2004), The Cocos and Carnegie aseismic ridges: A trace element record of long-term plume-spreading center interaction, *J. Petrol.*, *46*, 109–133, doi:10.1093/petrology/egh064.

Hart, S. R., and C. Brooks (1974), Clinopyroxene-matrix partitioning of K, Rb, Cs, and Ba, *Geochim. Cosmochim. Acta*, *38*, 1799–1806, doi:10.1016/0016-7037(74)90163-X.

Hauff, F., K. A. Hoernle, P. van den Bogaard, G. E. Alvarado, and D. Garbe-Schönberg (2000), Age and geochemistry of basaltic complexes in western Costa Rica: Contributions to the geotectonic evolution of Central America, *Geochem. Geophys. Geosyst.*, *1*(5), 1009, doi:10.1029/1999GC000020.

Herrstrom, E. A., M. K. Reagan, and J. D. Morris (1995), Variations in lava composition associated with flow of asthenosphere beneath southern Central America, *Geology*, *23*, 617–620, doi:10.1130/0091-7613(1995)023<0617:VILCAW>2.3.CO;2.

Herzberg, C. (2004), Geodynamic information in peridotite petrology, *J. Petrol.*, *45*(12), 2507–2530, doi:10.1093/petrology/egh039.

Hoernle, K. A., R. Werner, J. P. Morgan, J. Bryce, and J. Mrazek (2000), Existence of a complex spatial zonation in the Galápagos plume for at least 14.5 Ma, *Geology*, *28*, 435–438, doi:10.1130/0091-7613(2000)28<435:EOCSZI>2.0.CO;2.

Hoernle, K., P. van den Bogaard, R. Werner, B. Lissinna, F. Hauff, G. E. Alvarado, and D. Garbe-Schönberg (2002), Missing history (16–71 Ma) of the Galapagos hotspot: Implications for the tectonic and biological evolution of the Americas, *Geol. Soc. Am. Bull.*, *30*(9), 795–798.

Hoernle, K., F. Hauff, and P. van den Bogaard (2004), A 70 Myr history (139–69 Ma) for the Caribbean large igneous province, *Geology*, *32*, 697–700, doi:10.1130/G20574.1.

Hoernle, K., D. L. Abt, K. M. Fischer, H. Nichols, F. Hauff, G. A. Abers, P. van den Bogaard, G. Alvarado, M. Protti, and W. Strauch (2008), Arc-parallel flow in the mantle wedge beneath Costa Rica and Nicaragua, *Nature*, *451*, 1094–1097, doi:10.1038/nature06550.

Johnston, S. T., and D. J. Thorkelson (1997), Cocos-Nazca slab window beneath Central America, *Earth Planet. Sci. Lett.*, *146*, 465–474, doi:10.1016/S0012-821X(96)00242-7.

Kay, R. W. (1978), Aleutian magnesian andesites: Melts from the subducted Pacific Ocean crust, *J. Volcanol. Geotherm. Res.*, *4*, 117–132, doi:10.1016/0377-0273(78)90032-X.

Kelemen, P. B., H. J. B. Dick, and J. E. Quick (1992), Formation of harzburguite by pervasive melt/rock reaction in the upper mantle, *Nature*, *358*, 635–641, doi:10.1038/358635a0.

Kelemen, P. B., G. M. Yogodzinski, and D. Scholl (2003), Along-strike variation in the Aleutian island arc: Genesis of high Mg# andesites and implications for continental crust, in *Inside the Subduction Factory*, *Geophys. Monogr. Ser.*, vol. 138, edited by J. Eiler and G. Abers, pp. 223–276, AGU, Washington, D. C.

Kussmaul, S., J. Tournon, and G. E. Alvarado (1994), Evolution of the Neogene to Quaternary igneous rocks of Costa Rica, *Profil*, *7*, 97–123.

Lanphere, M. A., and G. B. Dalrymple (2000), First-principles calibration of ^{38}Ar tracers; implications for the ages of ^{40}Ar/^{39}Ar fluence monitors, *U.S. Geol. Surv. Prof. Pap.*, *1621*, 1–10.

Leeman, W. P., M. J. Carr, and J. D. Morris (1994), Boron geochemistry of the Central American arc: Constraints on the genesis of subduction-related magmas, *Geochim. Cosmochim. Acta*, *58*, 149–168, doi:10.1016/0016-7037(94)90453-7.

MacMillan, I., P. B. Gans, and G. Alvarado (2004), Middle Miocene to present plate tectonic history of the southern Central American volcanic arc, *Tectonophysics*, *392*, 325–348, doi:10.1016/j.tecto.2004.04.014.

Márquez, A., R. Oyarzun, M. Doblas, and S. P. Verma (1999), Alkalic (ocean-island type) and calc-alkalic volcanism in the Mexican volcanic belt: A case for plume-related magmatism and propagating rifting at an active margin?, *Geology*, *27*(1), 51–54, doi:10.1130/0091-7613(1999)027<0051:AOIBTA>2.3.CO;2.

Marshall, J. S., B. D. Idlemann, T. Garner, and D. M. Fisher (2003), Landcape evolution within retreating volcanic arc, Costa Rica, Central America, *Geology*, *31*(5), 419–422, doi:10.1130/0091-7613(2003)031<0419:LEWARV>2.0.CO;2.

McDonough, W. F., and S. S. Sun (1995), The composition of the Earth, *Chem. Geol.*, *120*, 223–253, doi:10.1016/0009-2541(94)00140-4.

Montelli, R., G. Nolet, F. A. Dahlen, and G. Masters (2006), A catalogue of deep mantle plumes: New results from finite-frequency tomography, *Geochem. Geophys. Geosyst.*, *7*, Q11007, doi:10.1029/2006GC001248.

Orozco-Esquivel, T., C. M. Petrone, L. Ferrari, T. Tagami, and P. Manetti (2007), Geochemical and isotopic variability in lavas from eastern Trans-Mexican volcanic belt: Slab detachment in a subduction zone with varying dip, *Lithos*, *93*, 149–174, doi:10.1016/j.lithos.2006.06.006.

Patino, L. C., M. J. Carr, and M. D. Feigenson (2000), Local and regional variations in Central American arc lavas controlled by variations in subducted sediment input, *Contrib. Mineral. Petrol.*, *138*, 265–283, doi:10.1007/s004100050562.

Peacock, S. M., P. E. van Keken, S. D. Holloway, B. R. Hacker, G. A. Abers, and R. L. Fergason (2005), Thermal structure of the Costa Rica-Nicaragua subduction zone, *Earth Planet. Sci. Lett.*, *149*, 187–200.

Plank, T., V. Balzer, and M. J. Carr (2002), Nicaraguan volcanoes record paleoceanographic changes accompanying closure of the Panama gateway, *Geology*, *30*, 1087–1090, doi:10.1130/0091-7613(2002)030<1087:NVRPCA>2.0.CO;2.

Ranero, C. R., and R. von Huene (2000), Subduction erosion along the Middle America convergent margin, *Nature*, *404*, 748–752, doi:10.1038/35008046.

Ranero, C. R., J. P. Morgan, K. McIntosh, and C. Reichert (2003), Bending-related faulting and mantle serpentinization at the Middle America trench, *Nature*, *425*, 367–373, doi:10.1038/nature01961.

Reagan, M. K., and J. G. Gill (1989), Coexisting of calc-alkaline and high-niobium basalts from Turrialba volcano, Costa Rica: Implications for residual titanites in arc magmas sources, *J. Geophys. Res.*, *94*, 4619–4633, doi:10.1029/JB094iB04p04619.

Reagan, M. K., J. D. Morris, E. A. Herrstrom, and M. T. Murrel (1994), Uranium series and beryllium isotope evidence for an extended history of subduction modification of the mantle below Nicaragua, *Geochim. Cosmochim. Acta*, *58*, 4199–4212, doi:10.1016/0016-7037(94)90273-9.

Russo, R. M., and P. G. Silver (1994), Trench-parallel flow beneath the Nazca plate from seismic anisotropy, *Science*, *263*, 1105–1111, doi:10.1126/science.263.5150.1105.

Sadofsky, S., M. K. Portnyagin, K. Hoernle, and P. van den Bogaard (2008), Subduction cycling of volatiles and trace elements through the Central American Volcanic Arc: Evidence from melt inclusions, *Contrib. Mineral. Petrol.*, *155*, 433–456, doi:10.1007/s00410-007-0251-3.

Shaw, D. M. (1970), Trace element fractionation during anatexis, *Geochim. Cosmochim. Acta*, *34*, 237–243, doi:10.1016/0016-7037(70)90009-8.

Silver, E., P. Costa Pisani, M. Hutnak, A. Fisher, H. DeShon, and B. Taylor (2004), An 8–10 Ma tectonic event on the Cocos Plate offshore Costa Rica: Result of the Cocos Ridge collision, *Geophys. Res. Lett.*, *31*, L18601, doi:10.1029/2004GL020272.

Thomsen, B. T., and M. W. Schmidt (2008), Melting of carbonated pelites at 2.5–5.0 GPa, silicate-carbonate liquid immiscibility, and potassium-carbon metasomatism of the mantle, *Earth Planet. Sci. Lett.*, *267*, 17–31, doi:10.1016/j.epsl.2007.11.027.

Tournon, J., and G. Alvarado (1997), *Mapa Geológico de Costa Rica*, Edit. Tecnol., Cartago, Costa Rica.

Vannucchi, P., D. M. Fisher, S. Bier, and T. W. Gardner (2006), From seamount accretion to tectonic erosion: Formation of Osa Mélange and the effects of Cocos Ridge subduction in southern Costa Rica, *Tectonics*, *25*, TC2004, doi:10.1029/2005TC001855.

Wendt, J. I., M. Regelous, K. D. Collerson, and A. Ewart (1997), Evidence for a contribution from two mantle plumes to island-arc lavas from northern Tonga, *Geology*, *25*(7), 611–614, doi:10.1130/0091-7613(1997)025<0611:EFACFT>2.3.CO;2.

Werner, R., K. Hoernle, P. van den Bogaard, C. Ranero, and R. von Hune (1999), Drowned 14 m.y.-old Galapagos archipelago off the coast of Costa Rica: Implications for tectonic and evolutionary models, *Geology*, *27*(6), 499–502, doi:10.1130/0091-7613(1999)027<0499:DMYOGP>2.3.CO;2.

Werner, R., K. Hoernle, U. Barckhausen, and F. Hauff (2003), Geodynamic evolution of the Galapagos hotspot system (central East Pacific) over the past 20 m.y.: Constraints from morphology, geochemistry, and magnetic anomalies, *Geochem. Geophys. Geosyst.*, *4*(12), 1108, doi:10.1029/2003GC000576.

Wiesemann, G. (1975), Remarks on the geologic structure of the Republic of El Salvador, Central America, *Mitt. Geol. Palaõnt. Inst. Univ. Hamburg*, *44*, 557–574.

Workman, R. K., and S. Hart (2005), Major and trace element composition of the depleted MORB mantle (DMM), *Earth Planet. Sci. Lett.*, *231*, 53–72, doi:10.1016/j.epsl.2004.12.005.